Clumped-isotope geothermometry and carbonate U–Pb geochronology of the Alta stock metamorphic aureole, Utah, USA: Insights on the kinetics of metamorphism in carbonates

Dana C. Brenner[1,*], Benjamin H. Passey[2], Robert M. Holder[1,2], Daniel R. Viete[1]

[1] *Department of Earth and Planetary Sciences, Johns Hopkins University, 3400 N Charles Street, Baltimore, MD 21218, USA;* [2] *Department of Earth and Environmental Sciences, University of Michigan, Ann Arbor, MI 48109, USA*

*Corresponding author: Dana Brenner (danabrenner@jhu.edu)

Key Points:

- Dolomite clumped isotopes record an abrupt ~180 °C decrease, over <50 meters, at the talc isograd of the Alta contact metamorphic aureole
- This step feature suggests strong thermal sensitivity in clumped-isotope reordering that precedes talc neocrystallization
- Clumped isotope geothermometry may provide new insights into processes controlling metamorphism and reaction kinetics in carbonates

This is the author manuscript accepted for publication and has undergone full peer review but has not been through the copyediting, typesetting, pagination and proofreading process, which may lead to differences between this version and the Version of Record. Please cite this article as doi: 10.1029/2020GC009238.

Abstract

To assess thermal and kinetic influences on atomic mobility and mineral (neo)crystallization, clumped-isotope abundances of calcite and dolomite were measured alongside dolomite cation ordering and U–Pb dates, across metamorphic grade within the c. 35–30 Ma Alta stock contact metamorphic aureole, Utah, USA. Average Δ_{47} values of dolomite inside the metamorphic aureole reflect the blocking temperature of dolomite (300–350 °C) during cooling from peak temperatures. Dolomite Δ_{47} values outside the metamorphic aureole record a temperature of ~160 °C. At the talc isograd, dolomite Δ_{47} values abruptly change, corresponding to a decrease of ~180 °C over <50 m in the down-temperature direction. This observed step in dolomite Δ_{47} values does not correlate with cation ordering in dolomite or U–Pb dates, neither of which correlate well with metamorphic grade. The short distance over which dolomite Δ_{47} values change indicates strong temperature sensitivity in the kinetics of dolomite clumped-isotope reordering, and is consistent with a wide range of clumped-isotope re-equilibration modeling results. We hypothesize that clumped-isotope reordering in dolomite precedes more extensive recrystallization or metamorphic reaction, such as the formation of talc. Dolomite U–Pb analyses from inside and outside the metamorphic aureole populate a single discordia ~60 Myr younger than depositional age (Mississippian), recording resetting in response to some older post-depositional, but pre-metamorphic process.

1. Introduction

Intrusion of magma into the near-surface (<15 km) environment produces localized heating and alteration (contact metamorphism) of upper-crustal rocks. Efforts to characterize the development of contact metamorphic aureoles have traditionally focused on high-temperature (>400 °C) alterations, involving precise mapping of the distribution of metamorphic products, geothermometry based on cation or stable isotope exchange, and/or numerical modeling (*e.g.*, Goldschmidt, 1911; Burnham, 1959; Kerrick, 1974; Masch & Heuss-Aßbichler, 1991; Ferry, 1996a, 1996b; Nabelek, 2007, 2009). The focus on high-temperature regions of metamorphic aureoles has partly related to difficulties in quantifying low-temperature (<400 °C) alterations. Clumped-isotope geothermometry is a relatively new technique that offers insight into such low-

temperature signatures, allowing a more complete reconstruction of thermal histories, spatially and temporally, associated with contact metamorphism (Ferry et al., 2011; Lloyd et al., 2017; Ryb et al., 2017).

The contact metamorphic aureole surrounding an igneous intrusion is generally defined by isograds (surfaces of constant metamorphic grade) observed in the field, which are characterized by up-grade first occurrence of an index mineral (minerals whose limited stability with respect to pressure and temperature make them useful for indicating degree of metamorphism). In contact metamorphism, isograds have traditionally been treated as markers of equilibrium pressure and temperature (*P–T*) conditions, representing preserved reaction fronts that propagated away from the intrusion as its heat and fluids were transferred to surrounding rocks. Such utilitarian approaches to studying metamorphic reactions have yielded great insight into drivers of metamorphism, including on the importance of fluid fluxes in carbonate systems (*e.g.*, Ferry, 1986). However, in regions that experienced extensive fluid infiltration, permeability structure can significantly influence metamorphic reactions (*e.g.*, Cook & Bowman, 2000). Furthermore, advances in understanding of non-equilibrium conditions for metamorphic reactions indicate that the attainment of pressures and temperatures necessary for equilibrium mineral crystallization (in a rock with all the appropriate reactants) only partially fulfills the requirement for an index-mineral-forming metamorphic reaction to occur. Index mineral formation also requires nucleation and growth, both of which can be inhibited by inefficient component exchange (*e.g.*, Carlson, 2002, 2006; Pattison & Tinkham, 2009; Pattison et al., 2011; George & Gaidies, 2020).

Studies into disequilibrium and partial equilibrium in metamorphic settings have focused on evidence from mineral growth patterns, composition, differing morphologies, and zonation in minerals, particularly in garnet, because its low elemental diffusivities and refractory nature allows for preservation of details lost during (re)crystallization of other minerals (Carlson, 2002; Ague & Carlson, 2013; Spear & Pattison, 2017; Beno et al., 2020). Carbonates are notoriously susceptible to alteration (Morse, 1983; Moore, 1989), meaning that records of processes involving disequilibrium or partial equilibrium in carbonates can be difficult to discern. In the absence of refractory minerals, changes within the carbonate matrix can provide insight into alterations that are otherwise cryptic.

Changes in carbonate clumped-isotope abundances can record solid-state, closed-system mobility of C and O atoms. Changes to carbonate U–Pb dates could indicate open-system processes (gain/loss of U or Pb) or closed-system recrystallization (re-distribution of U and Pb within the sample). Observations from both clumped isotopes and U–Pb data may offer insight into (re)crystallization histories, open- versus closed-system behavior, and disequilibrium or partial equilibrium in carbonates.

Carbonate clumped-isotope geothermometry and kinetic models of solid-state reordering have proven valuable in reconstructing thermal histories related to shallow crustal burial (*e.g.*, Henkes et al., 2014; Stolper & Eiler, 2015; Lacroix & Niemi, 2019) and have recently been applied to study the effects of low-grade metamorphism (Lloyd et al., 2017; Ryb et al., 2017). In this study we use carbonate clumped isotopes to investigate possible kinetic controls on metamorphism of silica-bearing carbonates in the Alta stock metamorphic aureole, Wasatch region of Utah, USA. The metamorphic aureole surrounding the Alta stock records a complex thermal history, involving significant advection of fluid and an unexpectedly prolonged duration of (re)crystallization (Cook & Bowman, 1994; Bowman et al., 1994; Cook et al., 1997; Bowman et al., 2009; Stearns et al., 2020). We investigate the thermal signatures recorded by carbon, oxygen, and clumped isotopes in calcite and dolomite of the Alta contact metamorphic aureole, and the extent to which clumped isotopes are able to capture upper-crustal thermal histories. Using insight gained from carbonate clumped-isotope geothermometry, U–Pb dating of carbonate, and dolomite cation ordering, we discuss potential kinetic requirements for index-mineral-forming metamorphic reactions. At Alta, we focus these efforts on the talc isograd, where abrupt changes in clumped-isotope values are observed.

1.1. Geologic background

The Wasatch Intrusive Belt (WIB) in North-central Utah hosts sedimentary rocks deposited during the Precambrian and Paleozoic that were subsequently buried (Baker et al., 1966; Cook & Bowman, 1994). Crustal thickening associated with the Sevier orogeny was followed by a series of igneous intrusions during the mid/late Paleogene. The eastern intrusions are oldest and shallowest, including the Valeo, Glencoe, Ontario,

Flagstaff, Pine Creek, Mayflower, and Park Premier stocks (Constenius, 1998; Vogel et al., 2001; Armstrong et al., 2003). Continuing westward, intrusions become progressively younger and deeper; the granodioritic Alta stock (35–30 Ma) partially intruded the older, granodioritic Clayton Peak stock (Baker et al., 1966; Cook & Bowman, 1994; Armstrong et al., 2003; Stearns et al., 2020). The Little Cottonwood stock, a granitoid body, is the youngest (36–25 Ma) and deepest-emplaced (6–11 km) WIB intrusion (Crittenden et al., 1965; Parry & Bruhn, 1986; John, 1989; Armstrong et al., 2003; Stearns et al., 2020). Recent *in situ* U–Pb zircon and titanite geochronology data from the Alta stock and its inner aureole suggest the Alta stock experienced prolonged, episodic hydrothermal activity (30–23 Ma) that overlapped emplacement of the Little Cottonwood stock (Stearns et al., 2020). Constraining the timing of these thermal events is an active area of research.

Eastward tilting and subsequent late Oligocene to present exhumation of the region to the east of the Wasatch Fault (axis of rotation ~25 km to the east) has resulted in subaerial exposure of the WIB intrusions (Wernicke & Axen, 1988; Armstrong et al., 2003; Ehlers et al., 2003; Friedrich et al., 2003). The pre-intrusive Alta–Grizzly thrust fault extends south of the Alta stock, and is associated with repetition of carbonate units within the study area (Baker et al., 1966; Cook & Bowman, 1994; Fig. 1a–b). The majority of the southern portion of the metamorphic aureole affected Cambrian and Mississippian carbonate rocks (Baker et al., 1966; Cook & Bowman, 1994, 2000; Cook et al., 1997).

Extensive study of the region has focused on addressing the spatial and temporal complexity of the thermal history surrounding the Alta stock, including the magnitude and direction of fluid flow during contact metamorphism and associated fluid-driven reactions (Bowman et al., 1994; Cook & Bowman, 1994, 2000; Ferry, 1994; Cook et al., 1997; Woodford et al., 2001; Bowman et al., 2009; Stearns et al., 2020). Metamorphism resulted in an isograd sequence of: talc (Tc, 350–400 °C, farthest from the stock), tremolite (Tr, 410–450 °C), forsterite (Fo, ~490 °C), clinohumite (Chm), and periclase (Per, ~580 °C, nearest the stock) (Moore & Kerrick, 1976; Cook & Bowman, 1994). The distribution of metamorphic isograds within the study area is shown in Fig. 1b.

In the periclase, forsterite, and tremolite zones, index minerals are widely distributed although abundances vary with stratigraphic horizon. Within the talc zone, the presence or absence of talc is more spatially restricted and highly bedding-specific (Cook & Bowman, 1994, 2000). Talc occurs primarily in reaction rinds around chert nodules in specific bedding planes, but bedding planes with unreacted chert nodules also occur (Cook & Bowman, 2000). Bedding control on the presence or absence of index minerals has been taken to suggest that fluid infiltration was stratigraphically controlled (Woodford, 1995; Cook & Bowman, 2000).

2. Materials and Methods

2.1. Samples and materials

This study focuses on Mississippian carbonate rocks of the southern portion of the metamorphic aureole. We preferentially sampled carbonates within the Deseret (Md, Upper Mississippian) and Gardison (Mg, Lower Mississippian) Formations, along a north–south transect extending ~3.5 km from the southern edge of the Alta stock, and in the western footwall of the Alta–Grizzly thrust fault (Fig. 1a). Two samples, AS17-33 and AS17-73,were collected from the Fitchville (Mf, Lower Mississippian) Formation and Maxfield Limestone (□m, Middle Cambrian), respectively, stratigraphically below the Deseret and Gardison Limestones (Fig. 1b; Table 1). High-grade alterations at Alta are well documented, including evidence for extensive fluid infiltration, changes to oxygen isotopic compositions, and varying crystal morphologies (Moore & Kerrick, 1976; Cook & Bowman, 1994; 2000; Cook et al., 1997; Beno et al., 2020). However, down-grade alterations are more cryptic when mineralogical based evidence for metamorphism is lacking (*e.g.*, in talc-absent beds at the talc isograd). The sampling strategy in this study was designed to evaluate changes in clumped-isotope abundances associated with thermal perturbation, but in the absence of macroscopic evidence of clear metamorphic reaction or fluid alteration. Therefore, sampling targeted unaltered, massive dolostone, when possible, avoiding areas of obvious recrystallization. The exceptions are samples AS17-68g, dolostone taken ~1cm from the reaction rind of a chert nodule (Fig. 2); AS17-73, dolostone taken <10cm from a bedding layer with abundant forsterite (Fig. S1); and AS17-74, calcitic marble in contact with the Alta stock. For all

analyses, small (~1 cm) pieces were taken from larger (~10 cm) hand samples, avoiding any prominent veins.

2.2. Carbonate stable and clumped-isotope analysis

2.2.1. Carbonate clumped-isotope geothermometry background

Carbonate clumped-isotope geothermometry is based on the isotopic exchange reaction:

$$X^{13}C^{18}O^{16}O_2 + X^{12}C^{16}O_3 \leftrightarrow X^{13}C^{16}O_3 + X^{12}C^{18}O^{16}O_2 \qquad (1)$$

where X represents a cation (*e.g.*, Ca, Mg). The equilibrium constant for Eq. (1) is temperature dependent; slight overabundance of the doubly-isotopically-substituted isotopologue (clumped isotope; containing both ^{13}C and ^{18}O) on the left side of Eq. (1) is energetically favored. This overabundance is relative to the abundance of clumped isotopes expected from a stochastic distribution of naturally occurring ^{13}C and ^{18}O, and the magnitude of the preference scales with temperature. A full explanation of the thermodynamic basis for preference of clumped isotopes is not provided here, and the reader is referred to Eiler and Schauble (2004), Wang et al. (2004), Ghosh et al. (2006), and Schauble et al. (2006) for detailed explanations.

The clumped-isotope composition of carbonate is measured by isotope ratio mass spectrometry of CO_2 gas produced from acid digestion of the carbonate. Carbonate clumped-isotope enrichment above stochastic (random) levels is expressed as:

$$\Delta_{47} = \left[\left(\frac{R^{47}}{R^{*47}} - 1\right) - \left(\frac{R^{46}}{R^{*46}} - 1\right) - \left(\frac{R^{45}}{R^{*45}} - 1\right)\right] \times 1000 \qquad (2)$$

where R^{*i} is the abundance ratio of the heavy isotopologue of mass *i* divided by the common isotopologue (mass 44), and the asterisk denotes a random distribution of isotopes among all isotopologues (Affek & Eiler, 2006).

In the absence of any type of thermal perturbation (*e.g.*, shallow crustal burial, contact metamorphism, shear heating, lightning strike), the clumped-isotope abundance

of carbonate minerals records the temperature of the last crystallization event. However, solid-state diffusion and isotopic exchange allow the clumped-isotope abundance of minerals to re-equilibrate partially or completely in response to heating (Dennis & Schrag, 2010; Passey & Henkes, 2012; Stolper & Eiler, 2015; Staudigel & Swart, 2016; Lloyd et al., 2017; Brenner et al., 2018; Chen et al., 2019). This process is referred to as solid-state clumped-isotope bond reordering. The precise mechanism of reordering is not well known, but it must involve the breaking and reforming of C and O bonds within carbonate groups of neighboring crystal lattice sites (Passey & Henkes, 2012; Henkes et al., 2014; Stolper & Eiler, 2015; Brenner et al., 2018), with the extent of reordering dependent on temperature and duration of the thermal perturbation. In other words, carbonates are in thermal equilibrium, and fully reordered, given sufficient time at a given temperature; for example, calcite held at ~400 °C is only completely reordered after ~10^5 yr (Brenner et al., 2018; see Fig. 7). However, even in scenarios where temperature varies temporally (*e.g.*, burial and exhumation), solid-state reordering may drive clumped-isotope abundances towards thermodynamic equilibrium. In a metamorphic scenario, equilibrium may be attained during prograde or early retrograde processes. Sustained decrease in ambient temperature during retrograde processes will eventually render clumped-isotopes to be effectively immobile. In this case, the measured isotopic composition records some apparent equilibrium 'blocking temperature', which is dependent on cooling rate and is analogous to the concept of 'closure temperature' in thermochronology (Dodson, 1973; Ferry et al., 2011; Passey & Henkes, 2012). The apparent equilibrium blocking temperature is higher for dolomitic than calcitic marbles—300–350 °C versus 150–200 °C, respectively, for cooling rates of 10^3–10^5 °C/Myr (Eiler, 2011; Ferry et al., 2011; Passey & Henkes, 2012; Lloyd et al., 2017; Ryb et al., 2017), suggesting more sluggish clumped-isotope re-equilibration kinetics for dolomite than calcite.

2.2.2. Carbonate stable isotope analytical methods

Samples were analyzed in the Stable Isotope Laboratory (SIL) and the Isotopologue Paleosciences Laboratory (IPL), both at the University of Michigan. Prior to acid digestion and analysis, all samples were crushed and powdered with an agate

mortar and pestle. Samples were analyzed in the SIL using a customized off-line vacuum line for CO_2 gas extraction and purification of all standards and unknowns, following the procedure of Defliese et al. (2015). Briefly, samples were digested in phosphoric acid (105 wt%, 90 °C) and the produced CO_2 gas was passed through two stages of cryogenic (-78 °C) purification, an Ag-wool getter, and one stage of Porapak Q (-20 °C) purification. Purified samples were sealed in gas sample vials for <12 hours prior to isotopic analysis. Samples were then analyzed for $\delta^{18}O$, $\delta^{13}C$, and Δ_{47} values on a Thermo-Finnigan MAT253 dual inlet mass spectrometer. Samples analyzed in the IPL used an automated preparation device (Passey et al., 2010) coupled to a Nu Perspective IS mass spectrometer operating in a high-resolution mode ($m/\Delta m$ ~3000). Briefly, samples were reacted in a common acid bath (100% H_3PO_4, 90 °C), and the produced CO_2 was purified by passage through multiple -78 °C cryogenic traps, an Ag-wool getter, and a -20 °C gas chromatography column (Porapak) prior to admittance into the mass spectrometer.

Samples with ≥98% dolomite or calcite, as measured by X-ray diffraction (XRD), were treated as monomineralic. For samples with mixed calcite–dolomite composition, pure calcite and pure dolomite components were isolated following the offline stepped acid digestion procedure of Lloyd et al. (2017). Briefly, samples were digested in phosphoric acid (100%) at 25 °C for 24 hours, with CO_2 collected in the first two hours considered to have originated primarily from the calcite component, and all gas produced in the 22 hours after the calcite collection discarded. After 24 hours of reaction at 25 °C, the sample was reacted at 50 °C for 24 hours and the produced gas collected was considered to have originated primarily from the dolomite component. All gas produced from stepped acid digestions was analyzed on the Nu Perspective IS mass spectrometer in the IPL at the University of Michigan.

In both laboratories, heated and equilibrated gases along with carbonate standards were routinely analyzed during isotopic analytical runs. All raw Δ_{47} values were calculated assuming the R^{13}_{PDB}, R^{18}_{VSMOW}, R^{17}_{VSMOW}, and triple oxygen isotope slope λ of Brand et al. (2010), as recommended by Daëron et al. (2016), and were normalized to heated gases (CO_2 heated to 1000 °C) and equilibrated gases (CO_2 equilibrated with water at 30 °C) using the carbon dioxide equilibrium scale (CDES) of Dennis et al.

(2011). All Δ_{47} values are reported in Table 1 as both 90 °C (CDES90) acid digestion following the recommendation of Bonifacie et al. (2017) and 25 °C (CDES25) acid digestion-equivalent values using the 90 °C versus 25 °C correction of 0.0823‰ or the 50 °C versus 25 °C correction of 0.0376‰, each recommended by Defliese et al. (2015). The supporting information contains comparison of average Δ_{47} values from SIL and IPL (Fig. S2; Table S2) and data for each replicate analysis (Table S1).

The choice of temperature calibration can change the calculated apparent clumped-isotope temperatures by tens of degrees in the temperature range of interest for this study (~150–400 °C). (Bonifacie et al., 2017; Passey & Henkes, 2012; Kluge et al., 2015; Stolper & Eiler, 2015; Lloyd et al., 2017). However, our interpretations focus on relative down-grade differences in clumped-isotope temperatures, rather than absolute clumped-isotope temperature values, and are not strongly influenced by these uncertainties. Table 1 shows dolomite apparent temperature calculated using both the theoretical calibration based on *ab-initio* calculations of Schauble et al. (2006) and the high-temperature dolomite-specific experimental calibration of Bonifacie et al. (2017). The two calibrations are in good agreement at lower temperature, whereas at higher temperature, the calibration of Bonifacie et al. (2017) yields higher temperature estimates (by ~10–50 °C). Therefore, figures, interpretations, and further reference to dolomite Δ_{47} calculated temperature is based on the *ab-initio* calculations of Schauble et al. (2006), adding the acid fractionation factor of 0.176‰ suggested by Bonifacie et al. (2017).

2.3. Mineralogical composition analytical methods

Prior to isotopic analysis, powder XRD analysis was performed on all samples to confirm sample mineralogical composition for clumped-isotope analysis. XRD analysis was done on a Philips PANalytical X'Pert X-ray diffractometer at the Johns Hopkins University (JHU). Samples were analyzed over a 2Θ range of 20–70 degrees (Cu K α) using a 45 kV and 40 mA beam, with a step size of 0.026 (°2Θ) and integration time of 7.14 seconds per step. Samples included calcite, dolomite, and minor silicates. Samples with ≥98% calcite or dolomite present were treated as monomineralic for clumped-isotope analysis. Percentages of calcite and dolomite for mixed samples were calculated using an internal calibration curve created from known mixtures of 100% dolomite and

100% calcite, using the intensity of main d_{104} reflection for calcite and dolomite (Tennant & Berger, 1957).

The ideal dolomite structure has alternating cation layers of Mg and Ca, and cation ordering within dolomite refers to the extent that Ca and Mg are distributed into the appropriate cation layer. The degree of cation disorder can be estimated from the XRD pattern intensity ratio for d_{015}/d_{110} superlattice reflections, where the 015 reflections represent the most intense ordering reflections and the 110 reflections have no *c*-axis contributions and thus no ordering reflections (Goldsmith & Graf, 1958; Reeder & Wenk, 1983; Kaczmarek & Sibley, 2007). The 006 reflections also have no contribution to ordering and can be used for estimating degree of ordering (Reeder & Wenk, 1983; Schultz-Güttler, 1986; Hammouda et al., 2011; Zucchini et al., 2012); however, 006 is a lower order basal reflection and thus not used here.

Energy dispersive X-ray spectra (EDS) and scanning electron microscopy (SEM) images were collected for all samples with U–Pb dates. Prior to analysis, all samples were carbon coated. EDS and SEM images were collected at JHU in the Materials Characterization and Processing Core Facility on a ThermoFisher Scientific Helios G4 UC Focused Ion Beam/Scanning Electron Microscope equipped with an EDAX Octane Elite EDS detector. All images and spectra were acquired at 15 keV and a beam current of 1.6 nA unless otherwise stated.

2.4. U–Pb dating analytical methods

Samples were analyzed in the Tectonics, Metamorphic Petrology, and Orogenesis (TeMPO) Laboratory at JHU. Rock fragments (~1 cm pieces) were analyzed in polished epoxy mounts using a Teldyne-Cetac Analyte G2 193 nm Excimer laser ablation system, with a double volume HelEx II cell, coupled to an Agilent 8900 quadrupole inductively-coupled-plasma mass spectrometer (LA-ICP-MS) with no gas in the collision cell. Samples were measured by spot analysis; each analysis consisted of a 30 s ablation at a repetition rate of 10 Hz with a fluence of 2 J/cm^2 and a square spot size of 130 μm. Analyte was carried from the laser to the mass spectrometer with He, using a 'squid' for signal smoothing. Masses 204, 206, 207, 208, 232, and 238 were measured with integration times of 0.1 s. Data were processed as recommended by Roberts et al. (2017,

2020). Baseline-subtraction and instrument drift corrections were made with the commercially-available Iolite (v. 4) software, using the U–Pb Geochronology data reduction scheme and the NIST612 glass standard as the primary reference material (re-measured every 10 analyses). Following initial data processing in Iolite, a mass-bias correction to the $^{238}U/^{206}Pb$ ratios of each analysis was made such that the lower intercepts of the Tera–Wasserburg discordia for two limestone secondary reference materials, measured as unknowns, were accurately reproduced: WC-1 (Roberts et al., 2017; expected: 254.4 ± 6.4 Ma; measured: 252.4 ± 5.8 Ma, 95% Confidence Interval (C.I.) of lower intercepts) and Duff Brown Tank limestone (Hill et al., 2016; expected: 64.04 ± 0.67 Ma; measured: 64.59 ± 0.86 Ma). The accuracy of carbonate U–Pb dates (probably ~ ± 3% at 95% C.I.) is currently limited by heterogeneity of available reference materials, such as WC-1, which exhibits ≥2.5% scatter about best-fit discordia (Roberts et al., 2017) as well as uncertainties surrounding differences in the ablation characteristics of different carbonate materials (Roberts et al., 2017, 2020). This limitation in method accuracy does not influence the results of this study, which are generally less precise than the estimated accuracy of the method.

Measurement uncertainties are reported as 2s (s-notation is used rather than σ-notation as recommended by Horstwood et al. (2016) to avoid confusion with the standard deviation), which comprises 2 standard error (SE) of the analysis with additional uncertainty propagated from the spline fit used in Iolite to correct for machine drift. Lower intercepts and initial $^{207}Pb/^{206}Pb$ ($^{207}Pb/^{206}Pb_i$) of Tera–Wasserburg U–Pb discordia were calculated using the linear regression algorithm of York (2004), as implemented in IsoplotR (Vermeesch, 2018) and are reported at 95% C.I. alongside the number of analyses (*N*), mean square of the weighted deviates (*MSWD*: a measure of scatter about the discordia; Wendt & Carl, 1991), and 'probability of fit' (*p: p* >0.05 indicates data are indistinguishable, within uncertainties, at 95% C.I.). The regression of all dolomite data approximate a single discordia, but with slight excess scatter, as indicated by *MSWD* = 2.8 and *p* = 0. The reported 95% C.I. of the lower-intercept dates were expanded by a factor of $\sqrt{MSWD}$ to account for this overdispersion (Vermeesch, 2018).

3. Results

3.1. Petrography and sample characterization

Sub-forsterite grade samples were mostly near-pure dolostones, comprised of fine-grained dolomite crystals with minor quartz ± calcite ± pyrite. Grain sizes of these samples do not vary with position in the contact aureole (Fig. 2). Demonstrably metamorphic minerals such as tremolite and talc are generally absent in the samples that were collected (Fig. S3–S15), despite the presence of appropriate reactants: dolomite + quartz. An exception to this is the observation of trace amounts of talc in one fine-grained dolostone (AS17-68g; Fig. S11) collected next to a calcite–talc reaction rind around a chert nodule (AS17-68w; Fig. S12) at the talc isograd.

Evidence for metamorphic reaction and metasomatism in dolostones within the forsterite isograd is pervasive. These dolostones are generally coarser-grained than the lower-grade dolostones, commonly contain demonstrably metamorphic minerals, such as forsterite and spinel, and are mineralogically heterogeneous down to the cm scale (Fig. S1, S3, S14). However, fine-grained massive dolostone similar to those observed outside the forsterite isograd are also present (Fig. S9). The interplay of metamorphic and metasomatic reaction is well illustrated by sample AS17-73, collected 0.5 km from the Alta stock. This sample is oolitic dolostone taken from the Maxfield Limestone. The outcrop consists of alternating bedding planes with oolitic dolostone and forsterite-rich dolostone (Fig. S1). Prolific calcite veins crosscut the dolostone; the contacts of these veins and their host rock are characterized by abundant forsterite and spinel (Fig. S3, S14).

3.2. Stable isotopes of carbonates

Stable isotope data, mineralogy, and associated apparent equilibrium temperatures are summarized in Table 1. Uncertainty is reported as 95% C.I. of replicate analyses after Fernandez et al. (2017) or as 1 σ for averages of multiple samples. Calcite Δ_{47} values within the metamorphic aureole vary significantly, ranging from 0.296 ± 0.005‰ (CDES90, 95% C.I.) at the contact (AS17-74) to 0.425 ± 0.010‰ (CDES90, 95% C.I.) 0.5 km away from the stock (AS17-73), corresponding to apparent equilibrium temperatures of $T(\Delta_{47}) = 257^{+30}_{-25}$ °C (95% C.I.) and 112^{+11}_{-10} °C (95% C.I.), respectively.

The Δ_{47} value of calcite from talc–calcite reaction rinds surrounding chert and dolomite nodules 1.4 km from the Alta stock (AS17-68w) is 0.366 ± 0.029‰ (CDES90, 95% C.I.), recording a maximum temperature of $T(\Delta_{47}) = 162^{+33}_{-27}$ °C (95% C.I.).

Dolomite Δ_{47} values for samples outside the isograd-defined metamorphic aureole, ≥1.6 km from the Alta stock, average 0.353 ± 0.022‰ (CDES90, 1 σ), corresponding to an average of $T(\Delta_{47})$ = 158 ± 25 °C (1 σ). In contrast, the Δ_{47} values of dolomitic samples <1.5 km from the Alta stock are significantly lower, averaging 0.260 ± 0.037‰ (CDES90, 1 σ), corresponding to a higher $T(\Delta_{47})$ of 342 ± 83 °C (1 σ). Between the talc and forsterite isograds, dolomite samples are fine-grained and lack evidence for prominent metamorphic reaction or metasomatism (Fig. S4, S10, S13). Within the forsterite isograd, metamorphic reaction and metasomatism are more pervasive. There, sample AS17-73 has the lowest $T(\Delta_{47})$ within the metamorphic aureole and contains a prominent calcite vein with abundant elongate forsterite crystals (Fig. S3). Excluding sample AS17-73, average dolomite $T(\Delta_{47})$ within 1.5 km of the stock is 367 ± 45 °C (1 σ). Within 1.5 km of the stock, calcite records, on average, $T(\Delta_{47})$ that is ~160 °C lower than $T(\Delta_{47})$ of dolomite.

Figure 3 compares results from the clumped-isotope geothermometry of this study to the Cc–Do geothermometry results of Cook and Bowman (1994). Dolomite clumped-isotope geothermometry of samples 0.7–1.5 km from the Alta stock, within the forsterite, tremolite, and talc zones, yield temperatures within error of the second-order polynomial fit to the Cc–Do Mg-solvus geothermometry results of Cook and Bowman (1994; Fig. 3). However, dolomite clumped-isotope geothermometry of samples ≤0.5 km from the Alta stock, from the middle of the forsterite zone through the periclase zone, yield $T(\Delta_{47}) = 166^{+141}_{-71} - 381^{+71}_{-54}$ °C (95% C.I.), significantly below the 485–575 °C calculated from the Cc–Do geothermometry data of Cook and Bowman (1994). Arguably the most striking feature of Fig. 3 is an abrupt change in $T(\Delta_{47})$ (~180 °C decrease, away from the Alta stock) at a distance from the Alta stock of 1.5–1.6 km. This break in clumped-isotope temperature occurs over a relatively confined spatial area (<50 m) and, interestingly, coincides with the position of the talc isograd.

Calcite and dolomite $\delta^{13}C$ and $\delta^{18}O$ values from this study are in agreement with previous studies (Cook et al., 1997; Bowman et al., 2009). Dolomite samples beyond the talc isograd (≥1.6 km from the Alta stock) show little variation in $\delta^{13}C$ or $\delta^{18}O$ values, averaging 2.53 ± 0.57‰ (VPDB, 1 σ) and 29.27 ± 2.24‰ (VSMOW, 1 σ), respectively (Fig. 4a–b). Both calcite and dolomite samples within 1.0 km of the Alta stock show variability in $\delta^{13}C$ and $\delta^{18}O$ values. Samples located 0.7 and 1.0 km from the Alta stock (AS17-33 and AS17-39, respectively) are relatively depleted in ^{13}C, whereas samples located 0.2, 0.4, and 0.5 km from the Alta stock (AS17-36, AS17-37b, and AS17-73, respectively) are relatively enriched in ^{13}C (Fig. 4a). Both calcite and dolomite show a poorly correlated linear trend (R^2 = 0.03 and 0.32, respectively) of increasing depletion in ^{18}O in the up-temperature direction, toward the Alta stock (Fig. 4b). However, there is no statistical difference in dolomite $\delta^{18}O$ values across the talc isograd. Overall, calcite samples are more depleted in both ^{13}C and ^{18}O than dolomitic samples at the same location, which is expected for calcite–dolomite fractionation; at thermodynamic equilibrium, dolomite $\delta^{13}C$ and $\delta^{18}O$ values are higher than coexisting calcite (Schauble et al., 2006; Horita, 2014; Lloyd et al., 2017). Dolomite $\delta^{18}O$ and Δ_{47} values and $\delta^{13}C$ and $\delta^{18}O$ values are decoupled, whereas calcite shows weak positive correlations for both $\delta^{18}O$ and Δ_{47} values (R^2 = 0.46) and $\delta^{13}C$ and $\delta^{18}O$ values (R^2 = 0.40; Fig. 4c–d). The sample most depleted in both ^{13}C and ^{18}O is the calcite at the Alta stock contact (AS17-74). The largest difference between $\delta^{13}C$ and $\delta^{18}O$ values of dolomite and calcite is at 1.4 km from the Alta stock, where calcite (from talc-bearing reaction rinds surrounding chert) and dolomite differ in $\delta^{13}C$ and $\delta^{18}O$ values by 2.3‰ and 7.4‰, respectively (Fig. 4; Table 1). Figure 2a–c shows photographs of chert nodules with and without talc reaction rinds.

3.3. Dolomite cation ordering

Sample mineralogy and dolomite cation ordering are reported in Table 1. The degree of dolomite cation ordering was found not to correlate with metamorphic temperature, dolomite $\delta^{18}O$ values, or Δ_{47} values (Fig. S16b–c).

3.4. U-Pb dating of carbonates

Figure 5 shows a Tera–Wasserburg diagram for the U–Pb isotope data obtained for calcite and dolomite. Eight fine-grained, near-pure, massive dolostones—collected from outside the contact aureole to just within the forsterite isograd—were analyzed (AS17-24, AS17-26, AS17-28, AS17-29, AS17-39, AS17-44, AS17-68g, and AS17-70; see Fig. 1b and Table 1 for sample locations and information). As described above, these samples lack evidence for metamorphic reaction or metasomatism. One calcite–talc reaction rind around a chert nodule at the talc isograd (AS17-68w) was also dated. The calcite–talc reaction rind yielded relatively gently-sloping discordia with large uncertainty (31.1 ± 42.2 Ma, 95% C.I.; MSWD = 1.5, p = 0.074, N = 20), consistent with the interpretation that these reaction rinds formed late, during contact metamorphism and associated hydrothermal activity at Alta (Stearns et al., 2020). However, the date is too uncertain to interpret more specifically, and we do not discuss it further.

Data from all dolomite samples—including AS17-68g, which contains trace talc and was collected adjacent to the dated calcite–talc reaction rind (AS17-68w)—populate a single discordia, with lower intercept of 264.4 ± 15.1 Ma (*MSWD* = 2.8, p = 0, N = 160). Any possible correlation with metamorphic grade or clumped-isotope abundances is smaller than can be distinguished within the uncertainties of the measurements. This date is significantly younger than the Late Mississippian depositional age for the original marine carbonates of the Deseret and Gardison Formations (Baker et al., 1966), but significantly older than emplacement of the Alta stock and associated metamorphism/metasomatism (36–23 Ma; Stearns et al., 2020).

4. Discussion

4.1. Possible explanations for the break in dolomite clumped-isotope data

Here we explore possible explanations for the abrupt ~180 °C change in apparent temperature observed in the dolomite Δ_{47} data at the talc isograd. Such a sharp thermal gradient is inconsistent with most conductive and advective fluid heating models for contact metamorphism (*e.g.*, Cook & Bowman, 1997). The change in dolomite Δ_{47} values is therefore interpreted to represent an 'apparent' thermal break, possibly relating

to differential fluid flow, metamorphic recrystallization, and/or the kinetics of atomic mobility in the dolomite crystal structure.

4.1.1. Is the abrupt change in dolomite Δ_{47} values a result of differential fluid flow?

In metasomatism dominated by porous flow and associated fluid advection, the break in dolomite Δ_{47} values could relate to flow patterns in the outer aureole, perhaps recording 'fluid leakage' from the system (*cf.*, Cook & Bowman, 2000). However, in the field, there are no indications of faulting, dikes, unconformities, confining layers, or other structural/lithological changes that could account for 'leakage' coincident with the observed change in dolomite Δ_{47} values. In addition, the massive dolostone samples targeted for this study generally lack evidence for metasomatic recrystallization. Thus, an explanation for the pattern of dolomite Δ_{47} values based solely on differential flow is improbable.

4.1.2. Does the step in dolomite Δ_{47} values mark a metamorphic recrystallization front?

A change in crystal size, texture, or fabric, or any other indicator of (re)crystallization between dolomites recording high and low temperature Δ_{47} values could help explain the transition in Δ_{47} values ~1.5 km from the Alta stock. Static recrystallization should result in grain coarsening and could more effectively (more completely) alter the $\delta^{18}O$, $\delta^{13}C$ and Δ_{47} composition of the mineral than by intracrystalline diffusional exchange. However, we observed no systematic difference in carbonate fabric or grain size in thin sections of the measured fine-grained dolostones relative to their position inside or outside the contact aureole (Fig. 2). There was minor evidence of 'hairline' veins filled with secondary calcite crystals in some samples, but these were avoided in dolomite clumped-isotope analysis. In contrast, sample AS17-73 from within the forsterite isograd shows clear evidence for metamorphic reaction and metasomatism (Fig. S1, S3, S14) and records distinctly lower $T(\Delta_{47})$ when compared to the overall step-pattern of the dolomite data. We therefore exclude this sample from our interpretations.

Depleted ^{13}C and $\delta^{18}O$ values in calcite could indicate open-system behavior with infiltrating fluids (Fig. 4c–d). However, similar evidence that might suggest fluid–rock interactions in the massive dolomites we targeted for this study is lacking. This suggests closed-system, solid-state reordering of dolomite Δ_{47} values occurred. Correlative changes in Δ_{47} and $\delta^{18}O$ values or Δ_{47} values and cation ordering would suggest dolomite recrystallization (Veillard et al., 2019). However, such correlations were not observed (Fig. 4d, S15c). Finally, dolomite U–Pb dates show no apparent variation with distance from the stock or Δ_{47} values (Fig. 5) as might be expected if the samples were variably recrystallized. From these lines of evidence, we do not interpret the step in Δ_{47} values to be indicative of a metamorphic recrystallization front.

4.1.3. Is the step in dolomite Δ_{47} values due to temperature-sensitive clumped-isotope solid-state reordering kinetics?

Given the lack of evidence for a metasomatic or metamorphic recrystallization front affecting our samples, we suggest that the most probable explanation for the abrupt change in dolomite Δ_{47} values at the talc isograd relates to clumped-isotope reordering kinetics. Dolomite clumped-isotope geothermometry may be extremely sensitive to temperature. High activation energy for C and O isotopic mobilization prevents clumped-isotope reordering in rocks that closely approach, but do not exceed, some temperature threshold. This threshold behavior has been repeatedly observed in laboratory-based solid-state reordering studies under controlled heating conditions (Passey & Henkes, 2012; Henkes et al., 2014; Stolper & Eiler, 2015; Brenner et al., 2018; Lloyd et al., 2018). The apparently narrow temperature range (<50 °C) over which dolomite Δ_{47} values change at Alta is consistent with the 'temperature threshold' effect implicit in the concept of a blocking temperature, and represents an energetic requirement for the reaction to proceed. At temperatures greater than the blocking temperature, C and O isotopes are sufficiently mobile that reordering can occur; however, at temperatures below the blocking temperature, these isotopes are effectively immobile. Once this energetic requirement is met, rapid reordering may progress by defect/vacancy migration (Passey & Henkes, 2012; Henkes et al., 2014), dissociation of clumped isotopes into neighboring singly-substituted isotopologues (Stolper & Eiler, 2015), or some other

cryptic mechanism(s). Moreover, reaction progress of clumped-isotope reordering is a function of both temperature and time, which, given the right temperature–time combinations, could act to accentuate further the step change observed in dolomite clumped isotopes. The apparent blocking temperature of dolomitic marbles is estimated to be 300–350 °C for cooling rates of 1 °C/kyr (Ferry et al., 2011; Lloyd et al., 2017; 2018). This agrees with the average dolomite apparent equilibrium temperatures for samples inside the talc isograd (342 ± 83 °C, 1 σ) and the temperature at the talc isograd (350–400 °C: Ferry, 1994; Cook & Bowman, 1994, Cook et al., 1997; Fig. 3), where the abrupt change in dolomite Δ_{47} values occurs.

Furthermore, dolomite $T(\Delta_{47})$ values are decoupled from the presence/absence of talc within the talc zone. Talc-absent horizons should record lower $T(\Delta_{47})$ if solid-state mobilization of C and O in dolomite, altering dolomite clumped-isotope abundances, is due to recrystallization in association with the talc-forming reaction. However, this was not observed. Horizons within the talc zone, both with talc (sample AS17-68g) and without talc (AS17-24), record $T(\Delta_{47})$ within error, 378^{+67}_{-51} °C (95% C.I.) and 389^{+71}_{-54} °C (95% C.I.), respectively (Table 1). This observation suggests dolomite clumped-isotope reordering is independent of talc neocrystallization.

There are two plausible explanations for the average $T(\Delta_{47})$ of 158 ± 25 °C (1 σ) recorded by all dolomitic samples beyond the talc isograd. First, samples greater than 1.6 km from the Alta stock may not preserve thermal signatures from the metamorphic event, but instead record prior (re)crystallization at ~160 °C. This could represent a background burial temperature of 5–5.5 km for a geothermal gradient of 30 °C/km, which is consistent with burial depth findings of previous studies of the Alta stock (Bryant and Nichols, 1990; Bryant, 1992). Dolomite beyond the talc isograd might not have experienced sufficient heating (in magnitude or duration) to allow clumped-isotope reordering. An alternative explanation is that samples beyond the talc isograd do not record equilibrium temperatures, but rather were only partially reordered during stock emplacement. The possibility of partial reordering is explored in Sections 4.2 and 4.3.

4.2. Solid-state clumped-isotope reordering kinetic modeling

In light of the above observations and interpretations, we investigate to what extent thermal and kinetic modeling can reproduce the abrupt change in dolomite Δ_{47} values observed at the talc isograd, ~1.5 km from the Alta stock (supporting information S1–2). The thermal model follows two-dimensional (2-D) conduction with heat advection by fluid flow (after Cook et al., 1997). We acknowledge that the thermal history of the Alta stock is more complicated than a single emplacement event and subsequent, passive cooling; instead, possibly involving incremental magma emplacement (and associated thermal pulses), and/or post-emplacement hydrothermal activity (Stearns et al., 2020). Three different clumped-isotope reordering kinetic models were applied to two thermal histories, extracted from the thermal model using different initial starting temperatures (160 °C and 100 °C along the sampling transect). The two thermal histories—based on 5–5.5 km burial depth (Wilson, 1961; John, 1989) and 30 °C/km geothermal gradient (Wilson, 1961; Kohler, 1979; Parry & Bruhn, 1986; Mayo & Loucks, 1995) (160 °C), and on the minimum temperature scenario of Cook & Bowman (1994) (100 °C)—result in a plausible range of temperatures for the talc isograd (350–400 °C; see Fig. 3) given uncertainties in fluid-composition and pressure. The clumped-isotope reordering kinetic models include: 1) the pseudo-first-order model of Passey and Henkes (2012); 2) the transient-defect/equilibrium-defect model of Henkes et al. (2014); and 3) the exchange–diffusion model of Stolper and Eiler (2015). All models use the dolomite kinetic parameters of Lloyd et al. (2018). The reader is referred to supporting information S1–2 for detailed information about these thermal and kinetic models.

Figure 6 shows modeled Δ_{47} values with distance from the Alta stock for various cooling times (following intrusion of the Alta stock) between 5,000 yr and 500,000 yr, for each of the kinetic models and initial (pre-emplacement) temperature conditions (160 °C and 100 °C). The most striking finding from the thermal and kinetic model simulations is that all clumped-isotope kinetic models implemented produce step-like transitions in dolomite Δ_{47} values, similar to the observed pattern of $T(\Delta_{47})$ (Fig. 6a–c,g–i). Furthermore, the break in dolomite Δ_{47} values is preserved throughout the exhumation history for all kinetic models (Fig. 6d–f,j–l). This stepped feature thus appears to be a natural consequence of the temporal evolution of the thermal pulse, and illustrates the temperature sensitivity (threshold behavior) of clumped-isotope reordering kinetics. The

exchange-diffusion model of Stolper and Eiler (2015) achieves the best fit to the data. Also of note is that the exchange–diffusion model predicts partially reordered dolomite Δ_{47} values at lower metamorphic grade than the talc isograd (Fig. 6f,l). This suggests dolomite Δ_{47} values beyond the talc isograd might record partial alteration associated with metamorphism, rather than earlier (re)crystallization at burial temperatures of ~160 °C.

The kinetic models fail to exactly reproduce final observed $T(\Delta_{47})$ within the inner aureole, underestimating observations (Fig. 6d–f,j–l), and the majority of kinetic models do not spatially align with the observed break in dolomite Δ_{47} values (Fig. 6a–c,g–i). These disparities may arise from incomplete knowledge of the thermal history before, during, and after the metamorphic event, inaccuracies in kinetic reordering models and parameters, and/or error in the Δ_{47}–T calibration. For example, the single-pulse conductive thermal models do not capture the complexity of the temperature history at Alta, which is not well constrained (Stearns et al., 2020), and the kinetic models are hindered by limited data and increased error associated with down-temperature extrapolation of experimental data (Bonifacie et al., 2017; Lloyd et al., 2018). In order to explain $T(\Delta_{47})$ >350 °C within the metamorphic aureole, published kinetic parameters require cooling rates of 10–100 °C/yr (Lloyd et al., 2018), which are geologically unreasonable for Alta. We used a Monte-Carlo approach to determine kinetic parameters that result in near-perfect fits between model predictions and the entire observed $T(\Delta_{47})$ profile (see supporting information S2; Fig. S21–S22), but these kinetic parameters are significantly outside of experimentally determined values. We therefore emphasize that the important finding from these models is not a precise reproduction of the down-grade pattern of clumped-isotope variation in dolomites surrounding the Alta stock, but rather the recognition of fundamental threshold behavior in the progress of clumped-isotope reordering in carbonates.

4.3. Kinetic drivers of metamorphic mineral forming reactions

4.3.1. Interpretation of carbonate clumped-isotope kinetics and implications for the formation of talc

Here we discuss factors influencing talc crystallization and growth, the talc isograd at the Alta stock, and insights gained from observed changes in dolomite Δ_{47} values at Alta. From the observations of this study, we hypothesize: 1) dolomite clumped-isotope reordering appears to be one of multiple kinetic processes that is linked to, but precedes, talc neocrystallization; and 2) kinetic inhibitions to nucleation and growth may be responsible for the presence or absence of talc in the talc zone at Alta.

A major question is whether the spatial alignment of the talc isograd and the abrupt change in dolomite Δ_{47} values is merely a coincidence, or indicates that mobility of C and O in dolomite (reflected by changes in clumped-isotope abundances) is a limiting factor to the formation of talc. Equilibrium talc crystallization requires appropriate *P–T* conditions, reactant availability, and kinetic permissibility. Previous studies indicate that appropriate *P–T* conditions for the formation of talc were present and hypothesize that the occurrence of talc was reactant limited—specifically, infiltration of H_2O along more permeable beds was a primary control on talc formation at Alta (Cook & Bowman, 1994, 2000). However, assuming the presence of H_2O as a pore fluid in all units, along with the observation of ubiquitous chert and disseminated quartz (Fig. 2, S5–S15), at least minor talc should have formed in all samples of this study (Cook & Bowman, 1994, 2000). We therefore explore the hypothesis that talc neocrystallization was kinetically inhibited in our samples.

The breakdown of dolomite to calcite during the formation of talc occurs *via* the reaction:

$$3Do + 4SiO_2 + H_2O = Tc + 3Cc + 3CO_2 \qquad (3)$$

Distinct processes involved in this reaction may include (introduction and) disassociation of H_2O, release of CO_2 from dolomite, cation migration and reordering within dolomite, Mg removal from dolomite, structural changes to the carbonate crystal lattice, and release of SiO_2 from its precursor host phase (here, primarily chert). These reaction steps are unlikely to occur simultaneously, and may not progress as a linear sequence of events. Furthermore, the kinetics and diffusional length-scales for each component may differ markedly.

Once the activation energy for clumped-isotope reordering is overcome (190–280 kJ/mol; Lloyd et al., 2018), the reordering process appears to proceed rapidly, as indicated by the narrow temperature range over which the observed step in dolomite Δ_{47} values occurs (threshold behavior). Based on observed dolomite clumped-isotope reordering in the absence of metamorphic minerals, in our samples, we suggest that this kinetic barrier must be overcome prior to larger-length scale reaction in the rocks, such as talc neocrystallization. Chen et al. (2019) posited a similar hypothesis—alteration to clumped-isotope abundances occurring before recrystallization—in association with the aragonite to calcite phase transition.

We therefore hypothesize that mobility of C or O (or both) in dolomite (as reflected by clumped-isotope reordering) is a limiting factor to completion of the talc-forming reaction (Eq. 3), and that the alignment of the step-like change in dolomite Δ_{47} values with the talc isograd is not coincidental. Evidence supporting this includes: 1) talc-bearing dolomite at the talc isograd (N = 1, AS17-68g) is reordered [$T(\Delta_{47}) = 378^{+67}_{-51}$ °C (95% C.I.); Fig. 2d–e, S11]; 2) talc-absent dolomite at the talc isograd (N = 1, AS17-24) is also reordered [$T(\Delta_{47}) = 389^{+71}_{-54}$ °C (95% C.I.); Fig. 2f–g, S5]; and 3) all dolomite (N = 8, samples >1.5 from the Alta stock) that are not reordered or partially reordered lack talc [$T(\Delta_{47})$ ~ 160 °C; Table 1; Fig. S4, S6–8]. We suggest that the abrupt change in dolomite clumped-isotope values represents a 'kinetic isograd'—*i.e.*, a thermally-controlled, isograd-like feature. This single-mineral 'kinetic isograd' is defined by an abrupt, down-grade change in the degree of internal isotopic ordering, and is unique in that does not require the presence of other reactants.

Furthermore, we hypothesize that the sporadic occurrence of talc at the talc isograd, despite widespread appropriate bulk-rock compositions, potentially reflects additional processes necessary for talc (neo)crystallization that are kinetically inhibited and may vary with lithology (see also George & Gaidies, 2020). It is possible that nucleation of talc at Alta required temperature in excess of that required for equilibrium talc crystallization, similar to the overstepping of the garnet-in reaction suggested to be necessary for nucleation of garnet porphyroblasts in some rocks (*e.g.*, Carlson, 2011; Pattison et al., 2011; Spear et al., 2014; Spear & Pattison, 2017). Even after the

activation energy to C–O reordering is overcome, talc crystallization may continue to have kinetic and/or reactant limitations.

4.3.2. Interpretation of combined clumped isotope and U–Pb datasets in dolomite

The U–Pb dating of sedimentary carbonates is still in its infancy, and the exact processes that are recorded by U–Pb dates in different geologic settings are not fully understood. Given the sensitivity of carbonate minerals to diagenesis and recrystallization, it is probable that U–Pb dates of carbonate rocks will commonly be reset from their original depositional age. The U–Pb dolomite dates presented here (c. 264 Ma) are homogeneous, substantially older than the age of contact metamorphism (c. 35–30 Ma), and ~60 Myr younger than depositional ages of the Deseret and Gardison Formations. The homogeneity of the dates, from well outside the isograd-defined contact aureole to the forsterite isograd (~500 °C), suggests that the dates were not strongly affected by metamorphism. This interpretation is further supported by the lack of evidence for significant metamorphic reaction in the dated samples.

These observations have two implications for understanding U–Pb dolomite dates. First, the diffusion of Pb and U was insufficient to modify the U–Pb dates of the samples during metamorphism, at least up to the forsterite isograd (~500 °C), even though grain size was relatively small (on the order of 100 µm). To a first order, this might indicate Pb diffusivity in dolomite is likely lower than in calcite, for which 100 µm Pb zoning is predicted to be significantly modified in rocks that reach ~375–400 °C for 0.1–1 Myr (Cherniak, 1997). A more precise empirical interpretation of dolomite Pb diffusivity and closure temperature is inhibited by the probable complexity of the Alta stock thermal history (Stearns et al., 2020) and permeability structure (Cook & Bowman, 2000), but this qualitative observation is valuable in that it suggests volume diffusion of Pb is unlikely to be significant in the sedimentary and low-temperature metamorphic environments to which U–Pb dolomite dating is most likely to be applied. Second, the dolomites appear to have been pervasively reset by some post-depositional process. We speculate that the c. 264 Ma date—approximately 60 Myr younger than deposition of the original marine carbonate—might reflect the timing of dolomitization, which requires appreciable open-system reaction and recrystallization (and therefore opportunity to reset

the U–Pb system). Alternatively, the date could reflect recrystallization associated with further burial or change in fluid compositions at some point after initial dolomitization occurred.

5. Summary and conclusions

Combining clumped-isotope geothermometry, U–Pb dating, and numerical modeling along with published Cc-Do geothermometry (Cook & Bowman, 1994), we investigate the temperature recorded in rocks subjected to contact metamorphism during intrusion of the Alta Stock, Utah, USA. Changes in $\delta^{13}C$ and $\delta^{18}O$ composition for calcite indicate interaction with magmatic fluids, in agreement with previous studies (Cook et al., 1997; Cook & Bowman, 2000).

Clumped-isotope geothermometry of dolomite samples >1.6 km from the Alta Stock records a consistent temperature of ~160 °C, potentially corresponding to ambient conditions at a burial depth of 5–5.5 km. At distances <1.5 km from the Alta Stock, clumped-isotope geothermometry of dolomite samples record contact-metamorphic thermal signatures (post-metamorphic cooling), with a maximum $T(\Delta_{47})$ of 422^{+84}_{-61} °C (95% C.I.). An abrupt change in dolomite Δ_{47} values occurs at the talc isograd (~1.5 km from the Alta Stock), corresponding to a decrease in apparent equilibrium temperature of ~180 °C over a distance of <50 m in the down-temperature direction. Two-dimensional thermal modeling (with fluid advection) and clumped-isotope reordering kinetic modeling are used to evaluate the origins of this stepped feature. Modeling results indicate that such features are a natural result of the down-grade evolution of thermally-activated C-O reordering in dolomites following a discrete heating event, such as that resulting from stock emplacement. Finally, factors influencing metamorphic mineral-forming reactions are explored, focusing on the talc isograd at Alta. We hypothesize that mobility of C or O (or both) in dolomite (as indicated by solid-state clumped-isotope reordering) may be a limiting factor for talc crystallization.

Isograds are traditionally considered demarcations of equilibrium *P*–*T* conditions defined by index minerals produced by metamorphic reactions. Analogously, the change in dolomite clumped-isotope abundances spatially represents a thermally-controlled isograd-like feature around Alta stock, but which is preserved within a single mineral,

independent of reaction with other minerals. In addition to its potential role as a 'kinetic isograd', clumped-isotope reordering may offer a useful tool for diagnosing kinetic drivers of mineral-forming reactions, and potential disequilibrium metamorphic scenarios in carbonates, in particular where other macroscopic (and microscopic) evidence is unavailable.

6. Acknowledgements

We are grateful to John Bowman for orientation and guidance in the field as well as helpful discussion related to the study. We thank Diego Berrios-Perez and Carl Beno for assistance with sample collection in the field. We thank Kacey Lohmann for the use of his Stable Isotope Laboratory and Sierra Peterson, Ian Winkelstern, and Kyle Meyer for assistance with clumped-isotope analysis. We are grateful to Ken Livi and Sam Norris for assistance with EDS and SEM analysis. We thank Max Lloyd for sharing his thermal model and clumped-isotope reordering model with us, and David Elbert for help with petrology. We are greatly appreciative of detailed and constructive comments by Michael Stearns and an anonymous reviewer that substantially improved the manuscript. Establishment of the LA-ICP-MS in the TeMPO Lab at JHU was supported by NSF Earth Sciences Instrumentation & Facilities (grant #1831766). This research was funded in part by JHU and the University of Michigan. Supporting information can be obtained at https://doi.org/10.7281/T1/VZZOJB.

7. References

Affek, H. P., & Eiler, J. M. (2006). Abundance of mass 47 CO_2 in urban air, car exhaust, and human breath. *Geochimica et Cosmochimica Acta*, *70*(1), 1–12. https://doi.org/10.1016/j.gca.2005.08.021

Ague, J. J., & Carlson, W. D. (2013). Metamorphism as garnet sees it: The kinetics of nucleation and growth, equilibration, and diffusional relaxation. *Elements*, *9*, 439–445. https://doi.org/10.2113/gselements.9.6.439

Armstrong, P. A., Ehlers, T. A., Chapman, D. S., Farley, K. A., & Kamp, P. J. J. (2003). Exhumation of the central Wasatch Mountains, Utah: 1. Patterns and timing of exhumation deduced from low-temperature thermochronology data. *Journal of*

Geophysical Research, 108(B3), 2172. https://doi.org/10.1029/2001JB001708

Baker, A. A., Calkins, F. C., Crittenden, M. D., & Bromfield, C. S. (1966). *Geologic map of Brighton quadrangle, Utah 7'5"* (Map GQ-534). Washington, DC: United States Geological Survey.

Beyssac, O., Pattison, D. R. M., & Bourdelle, F. (2018). Contrasting degrees of recrystallization of carbonaceous material in the Nelson aureole, British Columbia and Ballachulish aureole, Scotland, with implications for thermometry bassed on Raman spectroscopy of carbonaceous material. *Journal of Metamorphic Geology, 37*, 71–95. https://doi.org/10.1111/jmg.12449

Beno, C. J., Bowman, J. R., Loury P. C., Papanila, L. M., & Fernandez, D. P. (2020). Evidence for dendritic crystallization of forsterite olivine during contact metamorphism of siliceous dolostones, Alta stock aureole, Utah. *Contributions to Mineralogy and Petrology*, *175*(93), 1–26. https ://doi.org/10.1007/s0041 0-020-01734 -9

Bonifacie, M., Calmels, D. Eiler, J. M., Horita, J., Chaduteau, C., Vasconcelos, C., et al. (2017). Calibration of the dolomite clumped isotope thermometer from 25 to 350 °C, and implications for a universal calibration for all (Ca, Mg, Fe)CO_3 carbonates. *Geochimica et Cosmochimica Acta, 200*, 255–279. https://doi.org/10.1016/j.gca.2016.11.028

Bowman, J. R., Willett, S. D., & Cook, S. J. (1994). Oxygen isotopic transport and exchange during fluid flow: one-dimensional models and applications. *American Journal of Science, 294*, 1–55. doi: 10.2475/ajs.294.1.1

Bowman, J. R., Valley, J. W., & Kita, N. T. (2009). Mechanisms of oxygen isotopic exchange and isotopic evolution of $^{18}O/^{16}O$-depleted periclase zone marbles in the Alta aureole, Utah: insights from ion microprobe analysis of calcite. *Contributions to Mineralogy and Petrology, 157*, 77–93. https://doi.org/10.1007/s00410-008-0321-1

Brand, W., Assonov, S., & Coplen, T. (2010). Correction for the ^{17}O interference in $\delta^{13}C$ measurements when analyzing CO_2 with stale isotope mass spectrometry (IUPAC technical report). *Pure and Applied Chemistry, 82*, 1719–1733. doi: 10.1351/PAC-REP-09-01-05

Brenner, D. C., Passey, B. H., & Stolper, D. A. (2018). Influence of water on clumped isotope bond reordering kinetics in calcite. *Geochimica et Cosmochimica Acta, 224*, 42–63. https://doi.org/10.1016/j.gca.2017.12.026

Bryant, B., & Nichols, D. J. (1990). *Geologic map of the Salt Lake City 30' × 60' Quadrangle, north-central Utah, and Uinta County, Wyoming* (Map I-1944). Washington, DC: United States Geological Survey.

Bryant, B. (1992). *Geologic and structure maps of the Salt Lake City 1° × 2° Quadrangle, Utah and Wyoming* (Map I-1997). Washington, DC: United States Geological Survey.

Burnham, C. W. (1959). Contact metamorphism of magnesian limestones at Crestmore, California. *Geological Society of America Bulletin, 70*, 879–920. https://doi.org/10.1130/0016-7606(1959)70[879:cmomla]2.0.co;2

Carlson, W. D. (2002). Scales of disequilibrium and rates of equilibration during metamorphism. *American Mineralogist, 87*(2–3), 185–204. https://doi.org/10.2138/am-2002-2-301

Carlson, W. D. (2006). Rates of Fe, Mg, Mn, and Ca diffusion in garnet. *American Mineralogist, 91*(1), 1–11. https://doi.org/10.2138/am.2006.2043

Carlson, W. D. (2011). Porphyroblast crystallization: linking processes, kinetics, and microstructures. *International Geology Review, 53*(3–4), 406–445. https://doi.org/10.1080/00206814.2010.496184

Carslaw, H. S., & Jaeger, J. C. (1959). *Conduction of heat in solids* (2nd ed.). New York, NY: Oxford University Press.

Chen, S., Ryb, U., Piasecki, A. M., Lloyd M. K., Baker, M. B., & Eiler, J. M. (2019). Mechanism of solid-state clumped isotope reordering in carbonate minerals from aragonite heating experiments. *Geochimica et Cosmochimica Acta, 258*, 156–173. https://doi.org/10.1016/j.gca.2019.05.018

Cherniak, D. J. (1997). An experimental study of strontium and lead diffusion in calcite, and implications for carbonate diagenesis and metamorphism. *Geochimica et Cosmochimica Acta, 61*(19), 4773–4179. https://doi.org/10.1016/S0016-7037(97)00236-6

Constenius, K. N. (1998). *Extensional tectonics of the Cordilleran foreland fold and*

thrust belt and the Jurassic-Cretaceous Great Valley forearc basin (Doctoral dissertation). Retrieved from University of Arizona Campus Repository. (http://hdl.handle.net/10150/282601). Tuscon, AZ: University of Arizona.

Cook, S. J., & Bowman, J. R. (1994). Contact metamorphism surrounding the Alta stock: Thermal constraints and evidence of advective heat transport from calcite + dolomite geothermometry. *American Mineralogist, 79*, 513–525.

Cook, S. J., & Bowman, J. R. (2000). Mineralogical evidence for fluid-rock interaction accompanying prograde contact metamorphism of siliceous dolomites: Alta stock aureole, Utah, USA. *Journal of Petrology, 41*(6), 793–757. https://doi.org/10.1093/petrology/41.6.739

Cook, S. J., Bowman, J. R., & Forster, C. B. (1997). Contact metamorphism surrounding the Alta stock: Finite element model simulation of heat- and $^{18}O/^{16}O$ mass-transport during prograde metamorphism. *American Journal of Science, 297*(1), 1–55. https://doi.org/10.2475/ajs.297.1.1

Crittenden, M. D. (1965). *Geology of the Dromedary Peak quadrangle, Utah* (Map GQ-378). Washington, DC: United States Geological Survey.

Cui, X., Nabelek, P. I., & Liu, M. (2001). Heat and fluid flow in contact metamorphic aureoles with layered and transient permeability, with application to the Notch Peak aureole, Utah. *Journal of Geophysical Research, 106*(B4), 6477–6491. https://doi.org/10.1029/2000jb900418

Cui, X., Nabelek, P. I., & Liu, M. (2003). Reactive flow of mixed CO_2–H_2O fluid and progress of calc-silicate reactions in contact metamorphic aureoles: insights from two-dimensional numerical modeling. *Journal of Metamorphic Geology, 21*(7), 663–684. https://doi.org/10.1046/j.1525-1314.2003.00475.x

Daëron, M., Blamart, D., Peral, M., & Affek, H. (2016). Absolute isotopic abundance ratios and the accuracy of Δ_{47} measurements. *Chemical Geology, 441*, 83-96. https://doi.org/10.1016/j.chemgeo.2016.08.014

Defliese, W. F., Hren, M. T., & Lohmann, K. C. (2015). Compositional and temperature effects of phosphoric acid fractionation on Δ_{47} analysis and implications for discrepant calibrations. *Chemical Geology, 396*, 51–60. https://doi.org/10.1016/j.chemgeo.2014.12.018

Dennis, K. J., Affek, H. P., Passey, B. H., Schrag, D. P., & Eiler, J. M. (2011). Defining an absolute reference frame for 'clumped' isotope studies of CO_2. *Geochimica et Cosmochimica Acta, 75*, 7117–7131. https://doi.org/10.1016/j.gca.2011.09.025

Dennis, K. J., & Schrag, D. P. (2010). Clumped isotope thermometry of carbonatites as an indicator of diagenetic alteration. *Geochimica et Cosmochimica Acta, 74*, 4110–4122. https://doi.org/10.1016/j.gca.2010.04.005

Dodson, M. H. (1973). Closure temperature in cooling geochronological and petrological systems. *Contributions to Mineralogy and Petrology, 40*, 259–274. https://doi.org/10.1007/bf00373790

Ehlers, T. A., Willett ,S. D., Armstrong, P. A., & Chapman, D. S. (2003). Exhumation of the central Wasatch mountains, Utah: 2. Thermokinematic model of exhumation, erosion, and thermochronometer interpretation. *Journal of Geophysical Research, 108*(B3), 2173. https://doi.org/10.1029/2001jb001723

Eiler, J. M. (2011). Paleoclimate reconstruction using carbonate clumped isotope thermometry. *Quaternary Science Reviews*, 30(25–26), 3575–3588. https://doi.org/10.1016/j.quascirev.2011.09.001

Eiler, J. M., & Schauble, E. (2004). $^{18}O^{13}C^{16}O$ in Earth's atmosphere. *Geochimica et Cosmochimica Acta, 68*(23), 4767–4777. https://doi.org/10.1016/j.gca.2004.05.035

Fernandez, A. Müller, I. A., Rodríguez-Sanz, L., van Dijk J., Looser N., & Bernasconi S. M. (2017) A reassessment of the precision of carbonate clumped isotope measurements: implications for calibrations and paleoclimates reconstructions. *Geochemistry, Geosphysics, Geosystems, 18*, 4375–4386. https://doi.org/10.1002/2017GC007106

Ferry, J. M. (1986). Reaction progress: A monitor of fluid–rock interaction during metamorphic and hydrothermal events. In J. V. Walther & B. J. Wood (Eds.), *Fluid–rock interactions during metamorphism. Advances in physical geochemistry* (pp. 60–88). New York, NY: Springer.

Ferry, J. M. (1994). Role of fluid flow in the contact metamorphism of siliceous dolomitic limestone. *American Mineralogist, 79*, 719–736.

Ferry, J. M. (1996a). Prograde and retrograde fluid flow during contact metamorphism of siliceous carbonate rocks from the Ballachulish aureole, Scotland. *Contributions to Mineralogy and Petrology, 124*(3–4), 235–254. https://doi.org/10.1007/s004100050189

Ferry, J. M. (1996b). Three novel isograds in metamorphosed siliceous dolomites from the Ballachulish aureole, Scotland. *American Mineralogist, 81*(3–4), 485–494. https://doi.org/10.2138/am-1996-3-422

Ferry, J. M., Passey, B. H., Vasconcelos, C., & Eiler, J. M. (2011). Formation of dolomite at 40–80 °C in the Latemar carbonate buildup, Dolomites, Italy, from clumped isotope thermometry. *Geology, 39*(6), 571–574. https://doi.org/10.1130/g31845.1

Friedrich, A. M., Wernicke, B. P., Niemi, N. A., Bennett, R. A., & Davis, J. L. (2003). Comparison of geodetic and geologic data from the Wasatch region, Utah, and implications for the spectral character of Earth deformation at periods of 10 to 10 million years. *Journal of Geophysical Research, 108*(B4), 2199. doi:10.1029/2001JB000682

Furlong, K. P., Hanson, R. B., & Bowers, J. R. (1991). Modelling thermal regimes. In D. M. Kerrick (ed.), *Contact metamorphism* (Vol. 26, pp. 437–505). Washington, DC: Mineralogical Society of America.

George, F. R., & Gaidies, F. (2020). Simultaneous operation of opposing reaction mechanisms: The influence of matrix heterogeneity on post-kinematic garnet crystallization in an inverted metamorphic sequence. *Journal of Metamorphic Geology, 38*(7), 743–769. https://doi.org/10.1111/jmg.12539

Ghosh, P., Adkins J., Affek, H., Balta, B., Guo, W., Schauble, E. A., Schrag, D., & Eiler, J. M. (2006). $^{13}C–^{18}O$ bonds in carbonate minerals: a new kind of paleothermometer. *Geochimica et Cosmochimica Acta, 70*(6), 1439–1456. https://doi.org/10.1016/j.gca.2005.11.014

Goldschmidt, V. M. (1911). Die contact metamorphose im Kristianigebiet. In *Skrifter (Norske videnskaps-akademi. I-Mat.-Naturv.)* 1. Kristiania.

Goldsmith, J. R., & Graf D. L. (1958). Structural and compositional variations in some natural dolomites. *Journal of Geology, 6*(6), 678–693. https://doi.org/10.1086/626547

Hammouda, T., Andrault, D., Koga, K., Katsura, T., & Martin, A. M. (2011). Ordering in double carbonates and implications for processes at subduction zones. *Contributions to Mineralogy and Petrology, 161*(3), 439–450. https://doi.org/10.1007/s00410-010-0541-z

Hasterok, D., & Webb., J. (2017). On the radiogenic heat production of igneous rocks. *Geoscience Frontiers 8*, 919–940. https://doi.org/10.1016/j.gsf.2017.03.006

Hemingway, J. D. (2020). Isotopylog: Open-source tools for clumped isotope kinetic data analysis. http://pypi.python.org/pypi/isotopylog

Hemingway, J. D. & Henkes, G. A. (2020). A distributed activation energy model for clumped isotope bond reordering in carbonates. *Earth and Space Science Open Archive*. https://doi.org/10.1002/essoar.10504096.1

Henkes, G. A., Passey, B. H., Grossman, E. L., Shenton, B. J., Pérez-Huerta, A., & Yancey, T. E. (2014). Temperature limits for preservation of primary calcite clumped isotope paleotemperatures. *Geochimica et Cosmochimica Acta, 139*, 362–382. https://doi.org/10.1016/j.gca.2014.04.040

Hill, C. A., Polyak, V. J., Asmerom, Y., & Provencio, P. P. (2016). Constraints on a Late Cretaceous uplift, denudation, and incision of the Grand Canyon region, southwestern Colorado, Plateau, USA, from U–Pb dating of lacustrine limestone. *Tectonics, 35,* 896–906. https://doi.org/10.1002/2016TC004166

Horita, J. (2014). Oxygen and carbon isotope fractionation in the system dolomite-water-CO_2 to elevated temperatures. *Geochimica et Cosmochimica Acta, 129,* 111–124. https://doi.org/10.1016/j.gca.2013.12.027

Horstwood, M. S. A., Košler, J., Gehrels, G., Jackson, S. E., McLean, N. M., Paton, C., et al. (2016). Community-derived standards for LA-ICP-MS U-(Th-)Pb geochronology – Uncertainty propagation, age interpretation and data reporting. *Geostandards and Geoanalytical Research, 40*(3), 311–332. https://doi.org/10.1111/j.1751-908X.2016.00379.x

John, D. A. (1989). Geologic setting, depths of emplacement, and regional distribution of fluid includsions in intrusions of the central Wasatch Mountains, Utah. *Economic Geology, 84,* 386–409. https://doi.org/10.2113/gsecongeo.84.2.386

John, D. A. (1991). Evolution of hydrothermal fluids in the Alta tock, Central Wasatch Mountains, Utah. *U. S. Geological Survey Bulletin, 1977*. https://doi.org/10.3133/b1977

Kaczmarek, S. E., & Sibley, D. F. (2007). A comparison of nanometer-scale growth and dissolution features on natural and synthetic dolomite crystals: implications for the origin of dolomite. *Journal of Sediment Research, 77*(5), 242–432. https://doi.org/10.2110/jsr.2007.035

Kerrick, D. M. (1974). Review of metamorphic mixed-volatile (H_2O–CO_2) equilibria. *American Mineralogist, 59*, 729–762.

Kluge, T., John, C. M., Jourdan, A. -L., Davis, S., & Crawshaw, J. (2015). Laboratory calibration of the calcium carbonate lumped isotope thermometer in the 25–250 °C temperature range. *Geochimica et Cosmochimica Acta, 157*, 213–227. https://doi.org/10.1016/j.gca.2015.02.028

Kohler, J. F. (1979). Geology, characteristics, and resource potential of the low-temperature geothermal system near Midway, Wasatch County, Utah. *All U.S. Government Documents (Utah Regional Despository).* Paper 54.

Lacroix, B., & Niemi, N. A. (2019). Investigating the effect of burial histories on the clumped isotope thermometer: An example from the Green River and Washakie Basins, Wyoming. *Geochimica et Cosmochimica Acta, 247*, 40–58. https://doi.org/10.1016/j.gca.2018.12.016

Lange, R. A. (2003). The fusion curve of albite revisited and the compressibility of $NaAlSi_3O_8$ liquid with pressure. *American Mineralogist, 88*(1), 109–120. https://doi.org/10.2138/am-2003-0114

Lemmon, E. W., McLinden, M. O., & Friend, D. G. Thermophysical properties of fluid systems. In P. J. Linstrom & W. G. Mallard (Eds.), *NIST Chemistry WebBook, NIST Standard Reference Database Number 69* Gaithersburg, MD: National Institute of Standards and Technology. doi: 10.18434/T4D303

Lloyd, M. K. (2020). ClumpyCool. *Open Science Framework*. https://doi:10.17605/OSF.IO/JYHSW

Lloyd, M. K., Eiler, J. M., & Nabelek, P. I. (2017). Clumped isotope thermometry of calcite and dolomite in a contact metamorphic environment. *Geochimica et Cosmochimica Acta, 197*, 323–344. https://doi.org/10.1016/j.gca.2016.10.037

Lloyd, M. K., Ryb, U., & Eiler, J. M. (2018). Experimental calibration of clumped isotope reordering in dolomite. *Geochimica et Cosmochimica Acta, 242*, 1–20. https://doi.org/10.1016/j.gca.2018.08.036

Masch, L., & Heuss-Aßbichler, S. (1991). *Equilibrium and kinetics in contact metamorphism: The Ballachulish igneous complex and its aureole*, Berlin: Springer-Verlag.

Mayo, A. L., & Loucks, M. D. (1995). Solute and isotopic geochemistry and ground water flow in the central Wasatch Range, Utah. *Journal of Hydrology, 172*(1–4), 31–59. https://doi.org/10.1016/0022-1694(95)02748-e

Moore, C. H. (1989). Carbonate diagenesis and porosity. *Developments in sedimentology*. (Vol. 46). Amsterdam, The Netherlands: Elsevier Science.

Moore, J. N., & Kerrick, D. M. (1976). Equilibria in siliceous dolomites of the Alta aureole, Utah. *American Journal of Science, 276*(4), 502–542. https://doi.org/10.2475/ajs.276.4.502

Morse, J. W. (1983). The kinetics of calcium carbonate dissolution and precipitation. In R. J. Reeder (Ed.), *Carbonates: Mineralogy and chemistry*. (Vol. 26, pp. 227–264). Washington, DC: Mineralogical Society of America.

Nabelek, P. I. (2007). Fluid evolution and kinetics of metamorphic reactions in calc-silicate contact aureoles–From H_2O to CO_2 and back. *Geology, 35*(10), 927–930. https://doi.org/10.1130/g24051a.1

Nabelek, P. I. (2009). Numerical simulation of kinetically-controlled calc-silicate reactions and fluid flow with transient permeability around crystallizing plutons. *American Journal of Science, 309*(7), 517–548. https://doi.org/10.2475/07.2009.01

Nabelek, P. I., Hofmeister, A. M., & Whittington, A. G. (2012). The influence of temperature-dependent thermal diffusivity on the conductive cooling rates of plutons and temperature-time paths in contact aureoles. *Earth and Planetary Science Letters, 317–318*, 157–164. https://doi.org/10.1016/j.epsl.2011.11.009

Norton, D., & Cathles, L. M. (1979). Thermal aspects of ore deposition. In *Geochemistry of hydrothermal ore deposits* (Vol. 2, pp. 611–631). New York, NY: Wiley.

Parry, W. T., & Bruhn, R. L. (1986). Pore fluid and seismogenic characteristics of fault rock at depth on the Wasatch fault, Utah. *Journal of Geophysical Research, 91*(B1), 730–744. https://doi.org/10.1029/jb091ib01p00730

Passey, B. H., Levin, N. E., Cerling, T. E., Brown, F. H., & Eiler, J. M. (2010). High temperature environments of human evolution in East Africa based on bond ordering in paleosol carbonates. *Proceedings of the National Academy of Sciences of the United States of America, 107*(25), 11245–11249. https://doi.org/10.1073/pnas.1001824107

Passey, B. H., & Henkes, G. A. (2012). Carbonate clumped isotope bond reordering and geospeedometry. *Earth and Planetary Science Letters, 351–352*, 223–236. https://doi.org/10.1016/j.epsl.2012.07.021

Pattison, D. R. M., de Capitani, C., & Gaidies, F. (2011). Petrological consequences of variations in metamorphic reaction affinity. *Journal of Metamorphic Geology, 29*(9), 953–977. https://doi.org/10.1111/j.1525-1314.2011.00950.x

Pattison, D. R. M., & Tinkham, D. K. (2009). Interplay between equilibrium and kinetics in prograde metamorphism of pelites: an example from the Nelson aureole, British Columbia. *Journal of Metamorphic Geology, 27*(4), 249–279. https://doi.org/10.1111/j.1525-1314.2009.00816.x

Reeder, R. J., & Wenk, H. -R. (1983). Structure refinements of some thermally disordered dolomites. *American Mineralogist, 68*, 769–776.

Roberts, N. M. W., Drost, K., Horstwood, M. S. A., Condon, D. J., Chew, D., Drake, H., et al. (2020). Laser ablation inductively coupled plasma mass spectrometry (LA-ICP-MS) U–Pb carbonate geochronology: strategies, progress, and limitations. *Geochronology, 2*, 33–61. https://doi.org/10.5194/gchron-2-33-2020

Roberts, N. M. W., Rasbury, E. T., Parrish, R. R., Smith, C. J., Horstwood, M. S. A., & Condon, D. J. (2017). A calcite reference material for LA-ICP-MS U-Pb geochronology. *Geochemistry, Geophysics, Geosystems, 18*(7), 2807–2814. https://doi.org/10.1002/2016gc006784

Ryb, U., Lloyd, M. K., Stolper, D. A., & Eiler, J. M. (2017). The clumped-isotope

geochemistry of exhumed marbles from Naxos, Greece. *Earth and Planetary Science Letters, 470*, 1–12. https://doi.org/10.1016/j.epsl.2017.04.026

Schauble, E. A., Ghosh, P., & Eiler, J. M. (2006). Preferential formation of ^{13}C–^{18}O bonds in carbonate minerals, estimated using first-principles lattice dynamics. *Geochimica et Cosmochimica Acta, 70*(10), 2510–2529. https://doi.org/10.1016/j.gca.2006.02.011

Schultz-Güttler, R. (1986). The influence of disordered, non-equilibrium dolomites on the Mg-solubility in calcite in the system $CaCO_3$–$MgCO_3$. *Contributions to Mineralogy and Petrology, 93*(3), 395–398. https://doi.org/10.1007/bf00389397

Spear, F. S., & Pattison, D. R. M. (2017). The implications of overstepping for metamorphic assemblage diagrams (MADs). *Chemical Geology, 457*, 38–46. https://doi.org/10.1016/j.chemgeo.2017.03.011

Spear, F. S., Thomas, J. B., & Hallett, B. W. (2014). Overstepping the garnet isograd: a comparison of QuiG barometry and thermodynamic modeling. *Contributions to Mineralogy and Petrology, 168*(3), 1059. https://doi.org/10.1007/s00410-014-1059-6

Staudigel, P. T., & Swart, P. K. (2016). Isotopic behavior during the aragonite-calcite transition: Implications for sample preparation and proxy interpretation. *Chemical Geology*. *443*, 130–138. https://doi.org/10.1016/j.chemgeo.2016.09.013

Stearns, M. A., Bartley, J. M., Bowman, J. R., Forster, C. W., Beno, C. J., Riddle, D. D., Callis, S. J., & Udy, N. D. (2020). Simultaneous magmatic and hydrothermal regimes in Alta-Little Cottonwood stocks, Utah, USA, recorded using multiphase U-Pb petrochronology. *Geosciences, 10*(4), 129. https://doi.org/10.3390/geosciences10040129

Stolper, D. A., & Eiler, J. M. (2015). The kinetics of solid-state isotope-exchange reactions for clumped isotopes: A study of inorganic calcites and apatites from natural and experimental samples. *American Journal of Science, 315*(5), 363–411. https://doi.org/10.2475/05.2015.01

Taylor, H. P. (1974). The application of oxygen and hydrogen isotope studies to problems of hydrothermal alteration and ore deposition. *Economic Geology, 69*(6), 843–883. https://doi.org/10.2113/gsecongeo.69.6.843

Tennant, C. B., & Berger, R. W. (1957). X-ray determination of dolomite-calcite ratio of a carbonate rock. *American Mineralogist, 42*, 23–29.

Tenner, T. J., Lange, R. A., Downs, R. T. (2007). The albite fusion curve reexamined: new experiments and the high-pressure density and compressibility of high albite and $NaAlSi_3O_8$ liquid. *American Mineralogist, 92*, 1573–1585. https://doi.org/10.2138/am.2007.2464

Veillard, M. A., John, C. M., Krevor, S., & Najorka, J. (2019). Rock-buffered recrystallization of Marion Plateau dolomites at low temperature evidenced by clumped isotope thermometry and X-ray diffraction analysis. *Geochimica et Cosmochimica Acta, 252*, 190–212. https://doi.org/10.1016/j.gca.2019.02.012

Vermeesch, P. (2018). IsoplotR: a free and open toolbox for geochronology. *Geoscience Frontiers*. *9*(5), 1479–1493. https://doi.org/10.1016/j.gsf.2018.04.001

Vilà, M., Fernández, M., & Jiménez-Munt, I. (2010). Radiogenic heat production variability of some common lithological groups and its significance to lithospheric thermal modeling. *Tectonophysics, 490*(3–4), 152–164. https://doi.org/10.1016/j.tecto.2010.05.003

Vogel, T. A., Cambray, T.W., & Constenius, K.N. (2001). Origin and emplacement of igneous rocks in the central Wasatch Mountains, Utah. *Rocky Mountain Geology, 36*(2), 119–162. https://doi.org/10.2113/gsrocky.36.2.119

Wang, Z., Schauble, E. A., & Eiler, J. M. (2004). Equilibrium thermodynamics of multiply substituted isotopologues of molecular gases. *Geochimica et Cosmochimica Acta, 68*(23), 4779–4797. https://doi.org/10.1016/j.gca.2004.05.039

Watson, E. B., & Harrison, T. M. (1983). Zircon saturation revisited: Temperature and composition effects in a variety of crustal magma types. *Earth and Planetary Science Letters, 64*(2), 295–304. https://doi.org/10.1016/0012-821x(83)90211-x

Wendt, I., & Carl, C. (1991). The statistical distribution of the mean squared weighted deviation. *Chemical Geolology: Isotope Geoscience Section, 86*(4), 275–285. https://doi.org/10.1016/0168-9622(91)90010-t

Wernick, B., & Axen, G. J. (1988). On the role of isostasy in the evolution of normal fault systems. *Geology, 16*(9), 848–851. https://doi.org/10.1130/0091-

7613(1988)016<0848:otroii>2.3.co;2

Whittington, A. G., Hofmeister, A. M., & Nabelek, P. I. (2009). Temperature-dependent thermal diffusivity of Earth's crust and implications for magmatism. *Nature, 458*(7236), 319–321. https://doi.org/10.1038/nature07818

Wilson, J. W. (1961). *Geology of the Alta stock* (Doctoral dissertation). Retrieved from Caltech THESIS. (https://resolver.caltech.edu/CaltechTHESIS:04112011-153508154). Pasedena, CA: California Institute of Technology.

Woodford, D. T. (1995). *Boron metasomatism in the Alta stock thermal aureole, Alta, Utah* (Master's thesis). Retrieved from Rice University Electronic Theses and Dissertations. (https://hdl.handle.net/1911/14009). Houston, TX: Rice University.

Woodford D. T., Sisson V. B., & Leeman W. P. (2001). Boron metasomatism of the Alta stock contact aureole, Utah: Evidence from borates, mineral chemistry, and geochemistry. *American Mineralogist, 86*, 513–533. https://doi.org/10.2138/am-2001-0415

York, D., Evensen, N. M., Martínez, M. L., & De Basabe Delgado, J. (2004). Unified equations for the slope, intercept, and standard errors of the best straight line. *American Journal of Physics, 72*(3), 367–375. https://doi.org/10.1119/1.1632486

Zucchini, A., Comodi, P., Katerinopoulou, A., Balic-Zunic, T., McCammon, C., & Frondini, F. (2012). Order-disorder-reorder process in thermally treated dolomite samples: a combined powder and single-crystal X-ray diffraction study. *Physics and Chemistry of Minerals*, *39*(4), 319–328. https://doi.org/10.1007/s00269-012-0489-9

Table 1. Average values of $\delta^{18}O$, $\delta^{13}C$ and Δ_{47} for calcite and dolomite. Temperature calculated from clumped-isotope geothermometry shown with additional sample information.
Note: Reported uncertainty (± 95% C.I.) is the 95 percent confidence level of all replicates (*N*) of a single sample.
* Mf = Fitchville Formation, Mdg = Deseret and Gardison Formations, and □m = Maxfield Limestone.

† Values are reported in the carbon dioxide equilibrium scale (CDES) after Dennis et al. (2011), using both the 90 °C (CDES90) and 25 °C (CDES25) acid fractionation equivalent value.
‡ Temperature based on the universal calibration for calcite and the high temperature calibration for dolomite of Bonifacie et al. (2017).
§ Temperature based on the *ab initio* theoretical calculations specific to calcite or dolomite from Schauble et al. (2006).
|| Weight percent (wt. %) of either calcite or dolomite determined by XRD analysis, ≥98% one component unless otherwise stated.
Ordering refers to cation ordering in dolomite estimated from the intensity ratio of $d_{015}\backslash d_{110}$ reference peaks, measure from XRD patterns.

Figure 1. a) Geologic map of the Alta stock and surrounding area (modified after Cook and Bowman, 1994). Box indicates study area. Small insert shows location of the study area within Utah. b) Details of study area including sample locations (green stars) and prominent faults. Dotted white lines indicate approximate location of isograds: Per is periclase, Fo is forsterite, Tr is tremolite, and Tc is talc.

Figure 2. a–c) Photographs from the talc (Tc) isograd, ~1.5 km from the Alta stock. a) Chert nodule in dolostone with prominent Tc reaction rind surrounding the chert nodule. b) Same as (a) but Tc reaction rinds are absent from chert nodules. c) Same as (b) but chert nodule is significantly larger, dominating the left portion of the photograph, and Tc reaction rind appears to surround the dolostone located at the center of the photograph. d–i) Photomicrographs of fine-grained dolomite (Do) in cross polarized (d,f,h) and planar (e,g,i) light. d–e) Sample AS17-68g from horizon with Tc, 1.4 km from Alta Stock, $T(\Delta_{47})$ ~380 °C. f–g) Sample AS17-24 from horizon without Tc showing prominent calcite (Cc), 1.5 km from Alta Stock, $T(\Delta_{47})$ ~390 °C. h–i) Sample AS17-65, 3.6 km from Alta Stock, $T(\Delta_{47})$ ~160 °C. Py is pyrite. Scale bar in photomicrographs is 500 μm.

Figure 3. Clumped-isotope geothermometry results of this study and calcite-dolomite (Cc-Do) geothermometry results of Cook and Bowman (1994) plotted as a function of distance from the Alta stock. Open symbols represent Cc-Do geothermometry data of Cook and Bowman (1994). Closed symbols represent clumped-isotope replicate averages of this study; error bars represent 95% C.I. of replicate analyses. Clumped-isotope data are plotted as Δ_{47} values in the 90 °C carbon dioxide equilibrium scale (CDES90) of Dennis et al. (2011) on the right y-axis, and $T(\Delta_{47})$ using the theoretical temperature calibration of Schauble et al. (2006) for calcite and dolomite on the left y-axis. Vertical dashed lines indicate the approximate location of isograds. The black dashed and dotted curves represent peak temperature 100 kyr after initial pluton emplacement as calculated by a 2-D thermal model with an initial temperature (T_i) of 160 °C and 100 °C, respectively, for the sampling transect (see supporting information S1).

Figure 4. Calcite and dolomite $\delta^{13}C$, $\delta^{18}O$, and Δ_{47} values from this study. Error bars represent 95% C.I. for replicate analyses or are smaller than symbol size if absent. a)

$\delta^{13}C$ values plotted as a function of distance from the Alta stock. Symbols represent replicate averages from this study. Vertical dashed lines indicate the approximate location of isograds. b) Same as (a), but for $\delta^{18}O$ values and including data from Cook et al. (1997) as grey crosses. Calcite and dolomite c) $\delta^{13}C$ and $\delta^{18}O$ compositions for samples from this study and Cook et al. (1997) and d) $\delta^{18}O$ and Δ_{47} values for samples from this study. Open symbols represent data from Cook et al. (1997). Solid symbols represent replicate averages from this study. Colored background areas represent the $\delta^{18}O$ range for source fluids: marine and meteoric water (blue), magmatic fluids (red), and metamorphic fluids (yellow), after Ryb et al. (2017; see Fig. 4) and Taylor (1974).

Figure 5. Tera–Wasserburg diagram for U–Pb data of calcite and dolomite; orange data are calcite and blue data are dolomite. Calcite from a metamorphic reaction rind at the talc isograd (AS17-68w) gives an imprecise Cenozoic date, consistent with the timing of contact metamorphism and associated hydrothermal activity (36–23 Ma; Stearns et al., 2020). Dolomite dates are unambiguously older than metamorphism and are indistinguishable across metamorphic grade, but are younger than the depositional age of their precursor marine carbonate (Mississippian). Data uncertainties are plotted as 2s. Uncertainty on the calcite date is 95% C.I.; uncertainty on the dolomite date is 95% C.I. expanded by a factor of $\sqrt{MSWD}$ to account for slight overdispersion ($MSWD$ = 2.8, p = 0; Vermeesch, 2018).

Figure 6. a–c) Measured dolomite Δ_{47} values, plotted as a function of distance from the Alta stock (symbols), compared to modeled Δ_{47} values (curves) 5,000–500,000 yr after stock emplacement for sampling transect initial temperature (T_i) of 160 °C and Tc isograd maximum temperature (T_{max}) of 400 °C, using the kinetic parameters for dolomite of Lloyd et al. (2018): a) the pseudo-first-order model of Passey and Henkes (2012); b) the transient-defect model of Henkes et al. (2014); and c) the exchange-diffusion model of Stolper and Eiler (2015). Symbols represent replicate averages. Error bars represent 95% C.I. for replicate analyses or are smaller than symbol size if absent. Vertical dashed lines indicate the approximate location of isograds. d–f) Modeled $T(\Delta_{47})$ as a function of time (logarithmic scale) after emplacement of the Alta stock using the exhumation history of Armstrong et al. (2003). Curves represent distances from the Alta stock of 0.05–6.5 km. The dashed black curve represents the talc isograd. The grey region in d–f and j–l represents the $T(\Delta_{47})$ range of the metamorphic aureole. g–l) same as (a–f) except T_i = 100 °C and T_{max} = 350 °C. See supporting information S2 for modeling specifics.

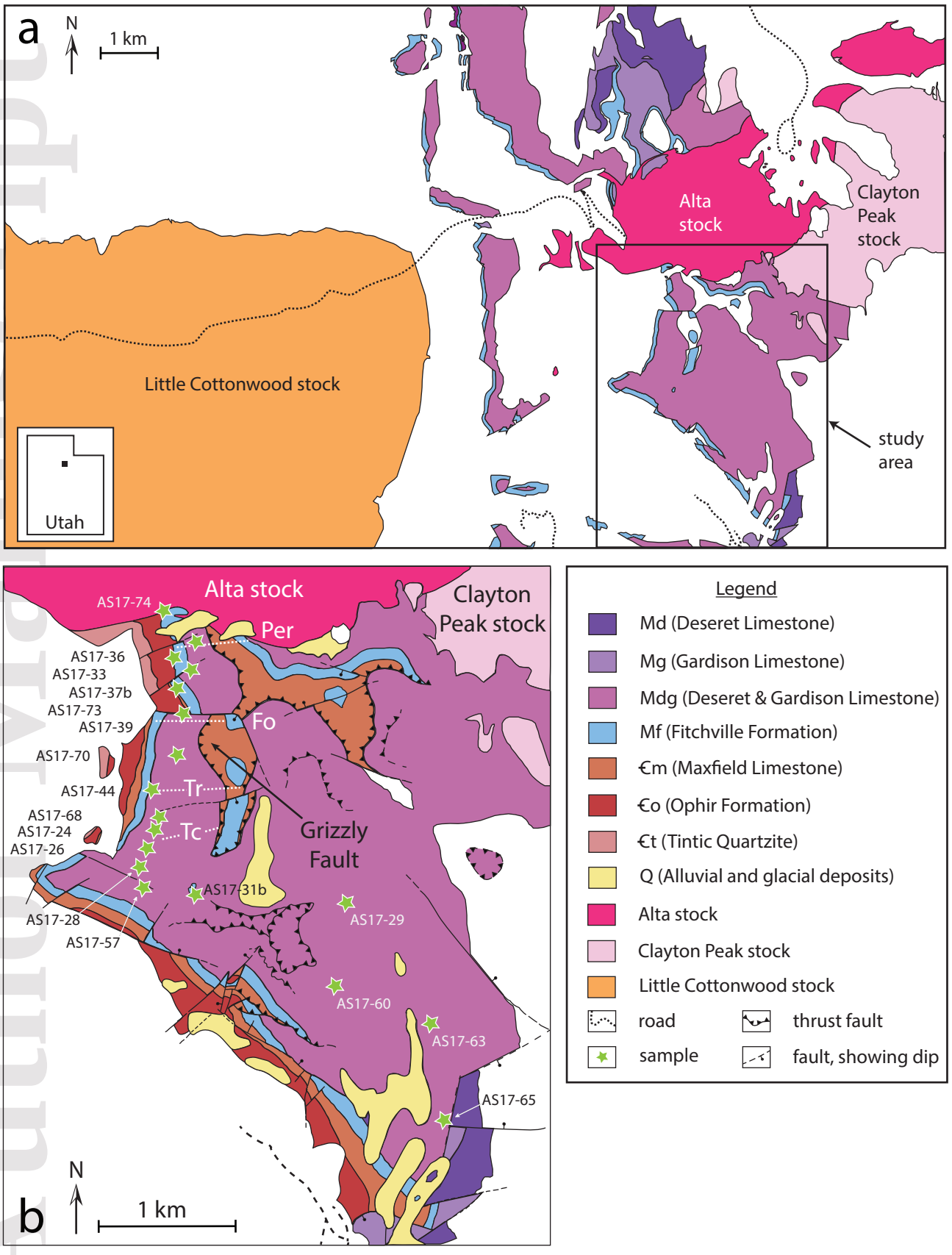

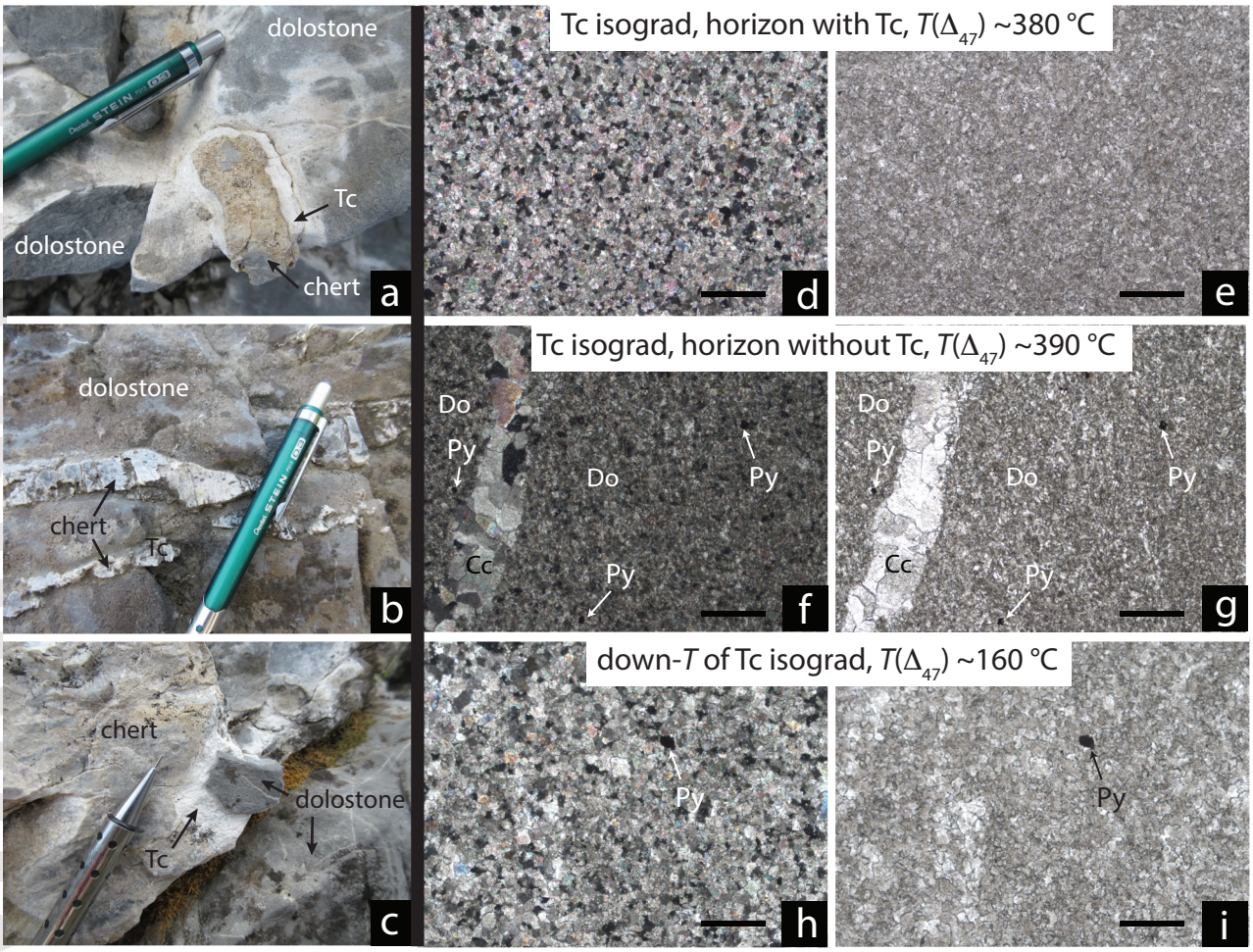

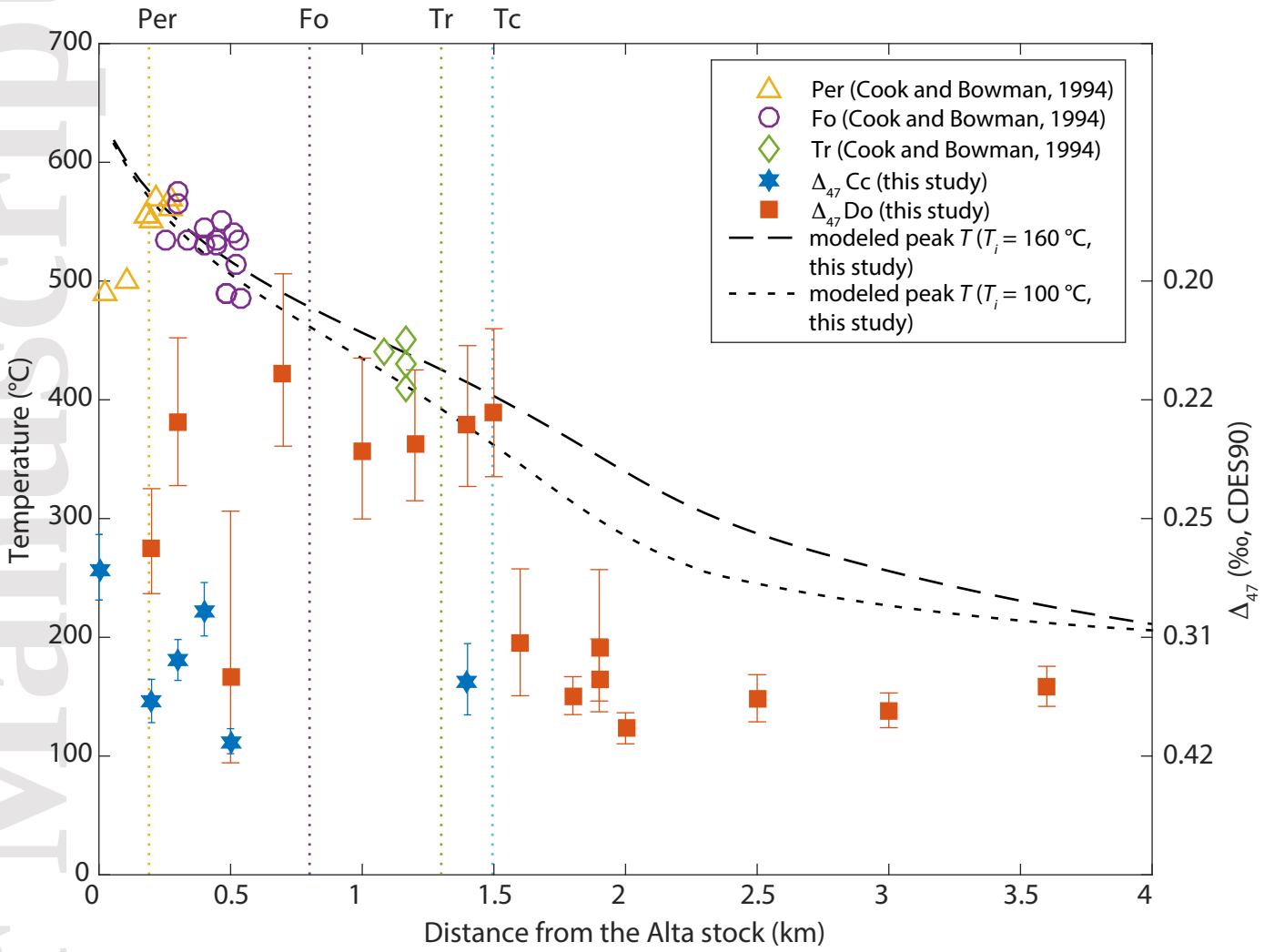

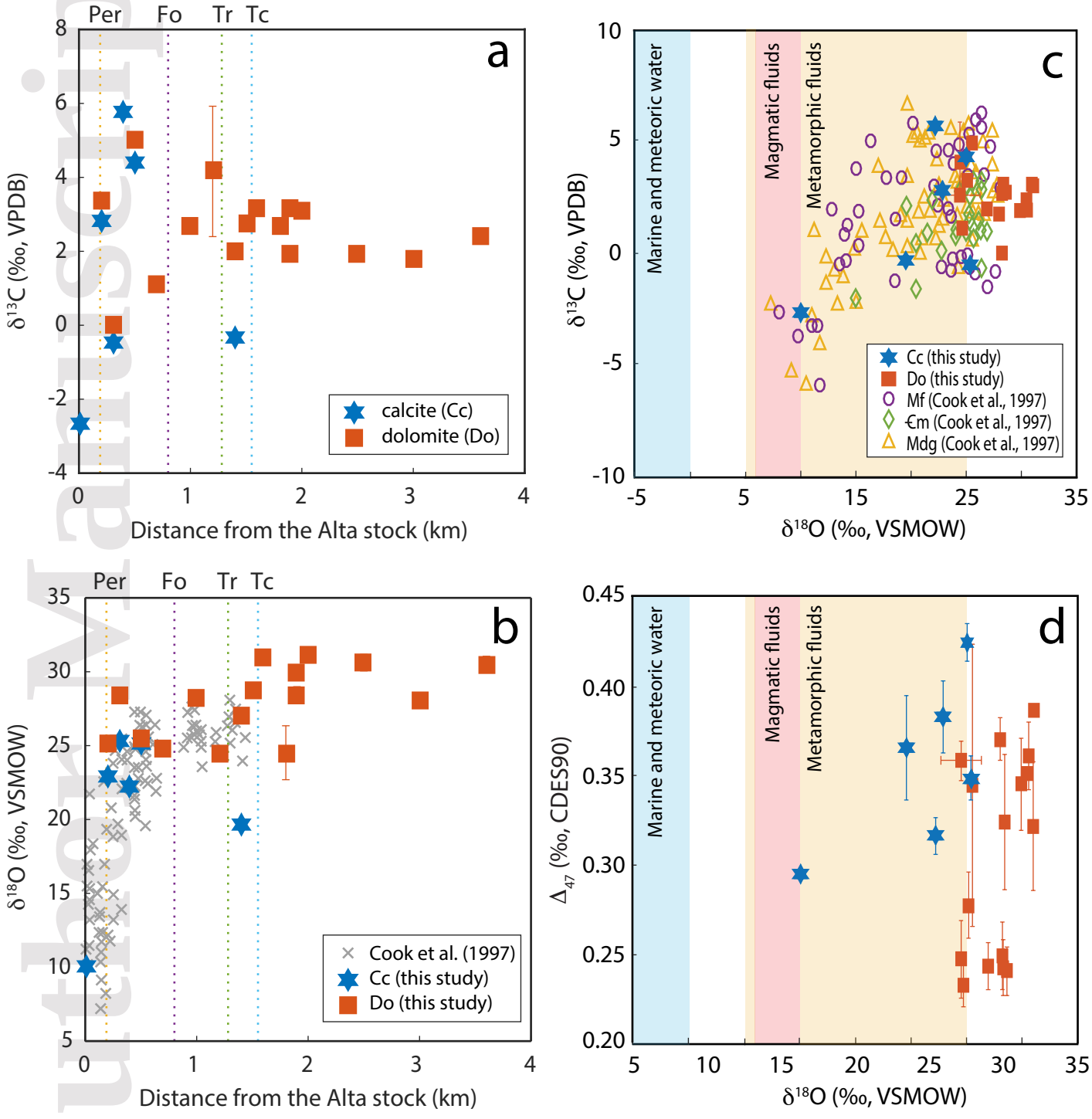

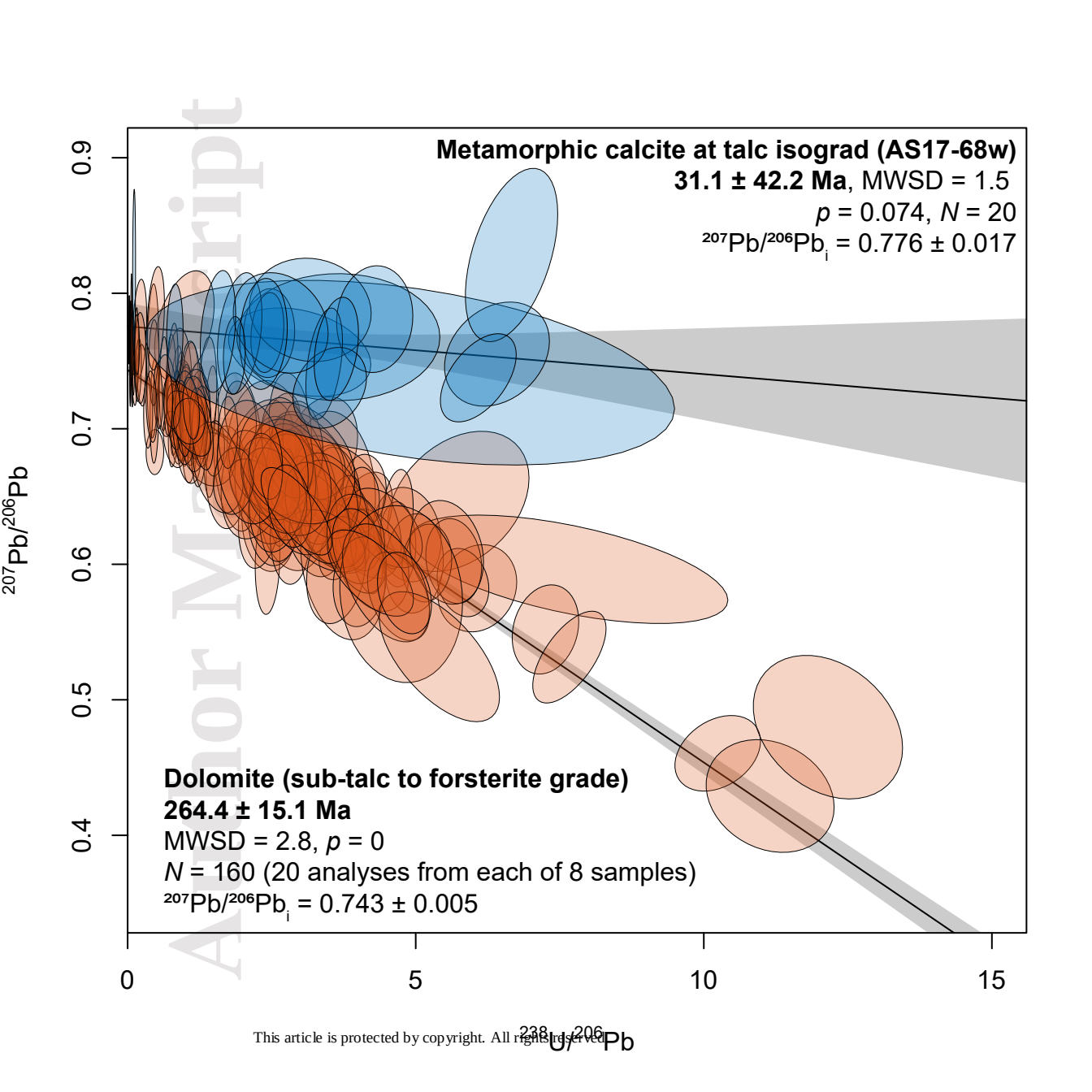

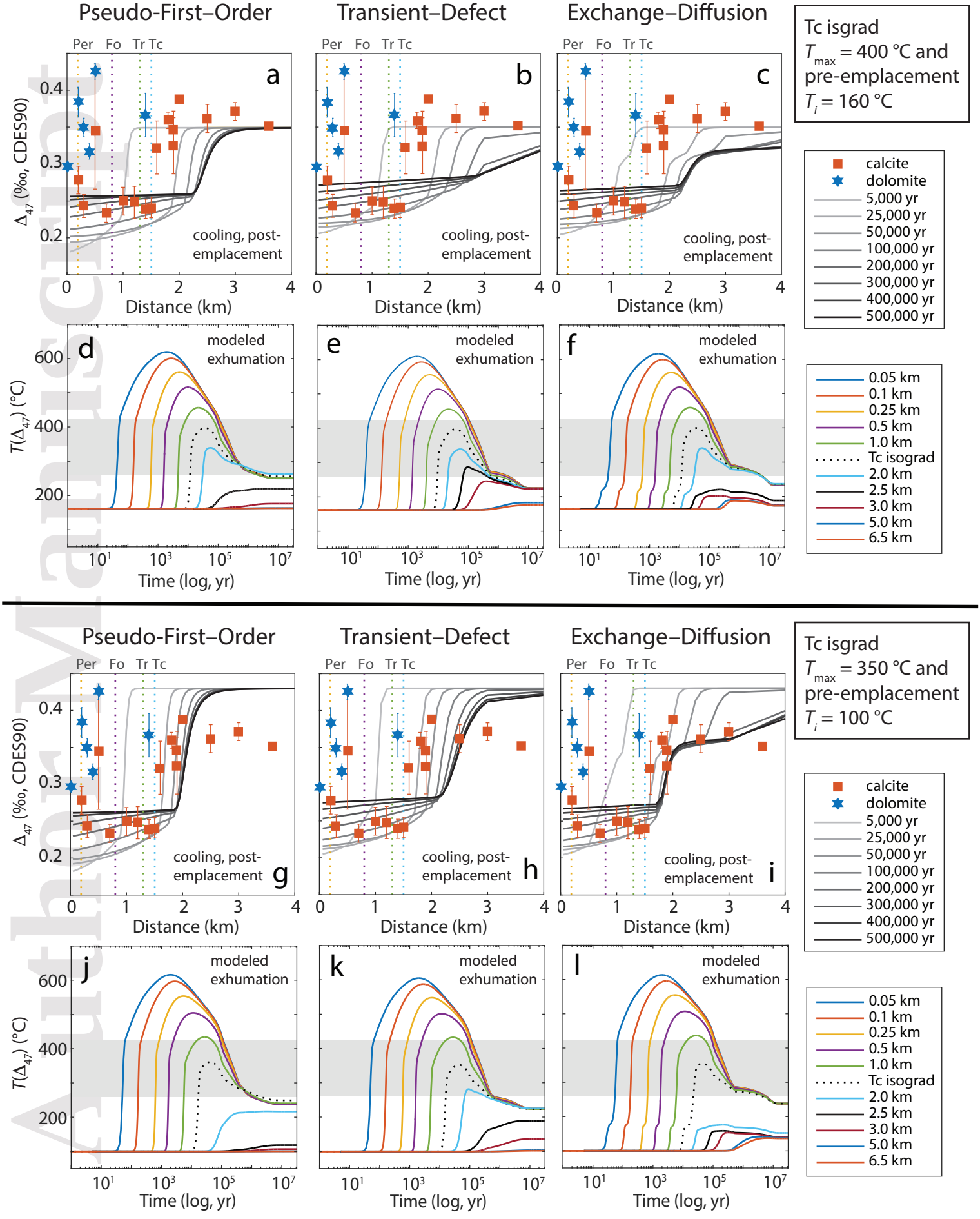

Sample	Dist. (km)	Fm*	*N*	$\delta^{13}C$ (‰) VPDB	$\delta^{18}O$ (‰) VSMOW	Δ_{47}† (‰) CDES90	Δ_{47}† (‰) CDES25	±95% C.I.	T‡ (°C)	T§ (°C)	+95% C.I.	-95% C.I.	Do/Cc‖ (wt. %)	Ordering#
calcite														
AS17-74	0.0	Mf	3	-2.63 ± 0.19	10.03 ± 0.55	0.296	0.378	0.005	225	257	30	25		
AS17-36-Cc	0.2	Mdg	2	2.85 ± 0.10	22.91 ± 0.15	0.384	0.466	0.020	132	145	19	17	20	
AS17-33-Cc	0.3	Mf	2	-0.47 ± 0.10	25.39 ± 0.15	0.349	0.432	0.013	162	180	18	16	15	
AS17-37b	0.4	Mdg	4	5.75 ± 0.13	22.21 ± 0.40	0.317	0.399	0.010	197	222	24	21		
AS17-73-Cc	0.5	□m	2	4.38 ± 0.10	25.09 ± 0.15	0.425	0.508	0.010	102	112	11	10	47	
AS17-68w	1.4	Mdg	5	-0.32 ± 0.07	19.57 ± 0.16	0.366	0.449	0.029	146	162	33	27		
dolomite														
AS17-36-Do	0.2	Mdg	2	3.34 ± 0.10	25.17 ± 0.15	0.278	0.361	0.019	299	276	49	39	80	1.06
AS17-33-Do	0.3	Mf	3	0.04 ± 0.08	28.32 ± 0.15	0.243	0.325	0.016	421	381	71	54	85	0.28
AS17-73-Do	0.5	□m	2	5.00 ± 0.10	25.53 ± 0.15	0.345	0.427	0.079	178	166	141	71	53	0.83
AS17-39	0.7	Mdg	5	1.14 ± 0.06	24.74 ± 0.20	0.233	0.316	0.012	471	422	84	61		0.82
AS17-70	1.0	Mdg	3	2.71 ± 0.08	28.23 ± 0.37	0.250	0.332	0.019	392	357	78	57		0.58
AS17-44	1.2	Mdg	3	4.16 ± 1.76	24.50 ± 0.23	0.248	0.330	0.022	400	363	62	48		0.41
AS17-68g	1.4	Mdg	4	2.03 ± 0.10	26.98 ± 0.31	0.244	0.326	0.013	418	378	67	51		0.62
AS17-24	1.5	Mdg	4	2.75 ± 0.07	28.68 ± 0.11	0.241	0.323	0.014	430	389	71	54		0.58
AS17-26	1.6	Mdg	3	3.14 ± 0.07	31.01 ± 0.23	0.322	0.405	0.036	210	195	62	45		0.77
AS17-28	1.8	Mdg	3	2.66 ± 0.08	24.52 ± 1.83	0.359	0.441	0.011	161	150	17	15		0.58
AS17-57	1.9	Mdg	2	3.14 ± 0.09	28.44 ± 0.55	0.325	0.407	0.038	207	192	65	46		0.64
AS17-31b	1.9	Mdg	2	1.96 ± 0.10	29.93 ± 0.46	0.346	0.428	0.026	177	165	34	27		0.64
AS17-29	2.0	Mdg	3	3.11 ± 0.08	31.10 ± 0.26	0.387	0.470	0.002	132	123	14	12		0.65
AS17-60	2.5	Mdg	2	1.96 ± 0.11	30.62 ± 0.56	0.362	0.444	0.019	158	147	21	18		0.79
AS17-63	3.0	Mdg	2	1.81 ± 0.10	28.03 ± 0.15	0.371	0.453	0.012	148	138	15	14		0.74
AS17-65	3.6	Mdg	2	2.44 ± 0.10	30.52 ± 0.53	0.352	0.401	0.002	170	158	18	16		0.60